



# Determining How Critical Zone Structure Constrains Hydrogeochemical Behavior of Watersheds: Learning From an Elevation Gradient in California's Sierra Nevada

OPEN ACCESS

**Edited by:**

Kamini Singha,  
Colorado School of Mines,  
United States

**Reviewed by:**

Matthys Alois Dippenaar,  
University of Pretoria, South Africa

Adam Wyman,  
University of New Hampshire,  
United States

Beth Hoagland,  
Colorado School of Mines,  
United States

**\*Correspondence:**

Julien Ackerer  
[julien.ackerer@orange.fr](mailto:julien.ackerer@orange.fr)

**Specialty section:**

This article was submitted to  
Water and Critical Zone,  
a section of the journal  
*Frontiers in Water*

**Received:** 23 March 2020

**Accepted:** 14 July 2020

**Published:** 21 August 2020

**Citation:**

Ackerer J, Steefel C, Liu F, Bart R, Safeeq M, O'Geen A, Hunsaker C and Bales R (2020) Determining How Critical Zone Structure Constrains Hydrogeochemical Behavior of Watersheds: Learning From an Elevation Gradient in California's Sierra Nevada. *Front. Water* 2:23.  
doi: 10.3389/frwa.2020.00023

Julien Ackerer<sup>1,2\*</sup>, Carl Steefel<sup>2</sup>, Fengjing Liu<sup>3</sup>, Ryan Bart<sup>1</sup>, Mohammad Safeeq<sup>1,4</sup>, Anthony O'Geen<sup>5</sup>, Carolyn Hunsaker<sup>6</sup> and Roger Bales<sup>1</sup>

<sup>1</sup> Sierra Nevada Research Institute, University of California, Merced, Merced, CA, United States, <sup>2</sup> Lawrence Berkeley National Laboratory, Berkeley, CA, United States, <sup>3</sup> College of Forest Resources and Environmental Science, Michigan Technological University, Houghton, MI, United States, <sup>4</sup> Division of Agriculture and Natural Resources, University of California, Davis, Davis, CA, United States, <sup>5</sup> Department of Land, Air and Water Resources, University of California, Davis, Davis, CA, United States, <sup>6</sup> Pacific Southwest Research Station, United States Forest Service, Fresno, CA, United States

Concentration-discharge (C-Q) relations can provide insight into the dynamic behavior of the Critical Zone (CZ), as C-Q relations integrate the spatial distribution and timing of watershed hydrogeochemical processes. This study blends geomorphologic analysis, C-Q relations and reactive-transport modeling using a rich dataset from an elevation gradient of eight watersheds in the Southern Sierra Nevada, California. We found that the CZ structure exerts a strong control on the C-Q relations, and on the hydrogeochemical behavior of headwater watersheds. Watersheds with thin regolith, a large stream network, and limited water storage have fast mean transit times along subsurface flow lines, and show limited seasonal variability in ionic concentrations in streamflow (i.e., chemostatic behavior). In contrast, watersheds with thicker regolith, a small stream network and more water storage have longer transit times along subsurface flow lines, and exhibit greater chemical variability (i.e., chemodynamic behavior). Independent estimates of mean transit times and water storage from other isotopic, hydrologic and geophysical studies were consistent with results from modeling C-Q relations. The stream chemistry and its variability were controlled by lateral flow within the regolith, and no mixing with deep groundwater was needed to explain the observed chemical variability. This study opens the possibility to estimate water-storage capacity and mean transit times, and thus drought resistance in watersheds, by using quantitative modeling of C-Q relations.

**Keywords:** critical zone, hydrogeochemical modeling, elevation gradient, watershed, C-Q relation

## INTRODUCTION

Improving our understanding of the critical zone (CZ), which is defined as the uppermost layer of Earth and is a key interface between the lithosphere, atmosphere, hydrosphere and biosphere, is important for predicting future soil and water societal issues. One of the most important questions in CZ science is what are the links and feedbacks between long-term CZ evolution (i.e., soil and regolith mineralogy, CZ structure and thickness) and the short-term hydrogeochemical behavior of watersheds (i.e., water availability, stream chemistry and water storage). This question is raised by the growing need for accurate estimates for water storage capacity and water transit times in watersheds, which are central to understanding water availability, water quality and drought responses (Hubbert et al., 2001; Bart and Hope, 2014; Safeeq and Hunsaker, 2016; Bales et al., 2018; Klos et al., 2018; O'Geen et al., 2018; Visser et al., 2019). How regolith structure and landscape evolution influence the hydrochemical behavior of watersheds depends on multiple physical, chemical and biological processes (Chorover et al., 2011; Ackerer et al., 2016; Reis and Brantley, 2019). Depicting how these processes are linked will depend on our ability to cross long-term monitoring efforts and the development of integrative modeling approaches (Steefel et al., 2015; Brantley et al., 2017; Li et al., 2017; Ackerer et al., 2018).

One promising approach to link CZ structure with the spatial distribution and timing of hydrogeochemical processes in watersheds is the quantitative interpretation of Concentration–Discharge (C-Q) relations (e.g., Godsey et al., 2009; Chorover et al., 2017; Moatar et al., 2017; Diamond and Cohen, 2018; Zhi et al., 2019). C-Q relations from stream water are acknowledged to aggregate a large number of processes, from climate, geochemical and ionic exchange reactions to hydrologic, biological and transport processes (Chorover et al., 2017). Recent reports show that C-Q relations can provide constraints on water flow paths along hillslopes (Ameli et al., 2017), mixing of different water end members in rivers (Liu et al., 2017; Torres et al., 2017) or seasonal variability of water transit times in headwater watersheds (Ackerer et al., 2018). There are ongoing debates around the extent to which C-Q relations are controlled by mixing between deep and shallow waters (Kim et al., 2017), synchronous dissolution of clay minerals (Li et al., 2017) and/or seasonally variable flow paths (Herndon et al., 2018).

Although C-Q relations have been intensively studied, few studies have coupled reactive-transport modeling, geomorphological investigations and regolith sciences to clearly assess what are the main CZ attributes that control the shapes of C-Q relations. Recent reports indicate that landscape heterogeneities are an important determinant of C-Q relations (e.g., Herndon et al., 2015; Musolff et al., 2015; Wymore et al., 2017; Sullivan et al., 2019). Understanding the specific roles of regolith thickness, bedrock geochemistry and watershed structures is an important new step to use C-Q relations to gain insight into water storage and water availability across landscapes. A detailed knowledge on how CZ structure controls the hydrogeochemical behavior of watersheds is also needed to anticipate the response of watersheds to perturbations from

global warming, because this response will rely on regolith properties acquired through its long-term evolution (Bales et al., 2011; Safeeq et al., 2013; O'Geen et al., 2018).

The major objectives of the research reported here were to determine: (a) how the CZ structure constrains the hydrogeochemical behavior of watersheds, and (b) how the variability of bedrock geochemistry and regolith thickness can impact stream water chemistry, mean transit times and water storage in headwater watersheds. Our hypotheses were that the features of subsurface flow lines and stream networks, together with the regolith thickness, have a strong control on the stream water chemistry and hydrological behavior of watersheds. To evaluate these points, our work combines a detailed analysis of geomorphic features, C-Q relations, and reactive-transport modeling in eight headwater watersheds along a unique elevation gradient in California's Sierra Nevada.

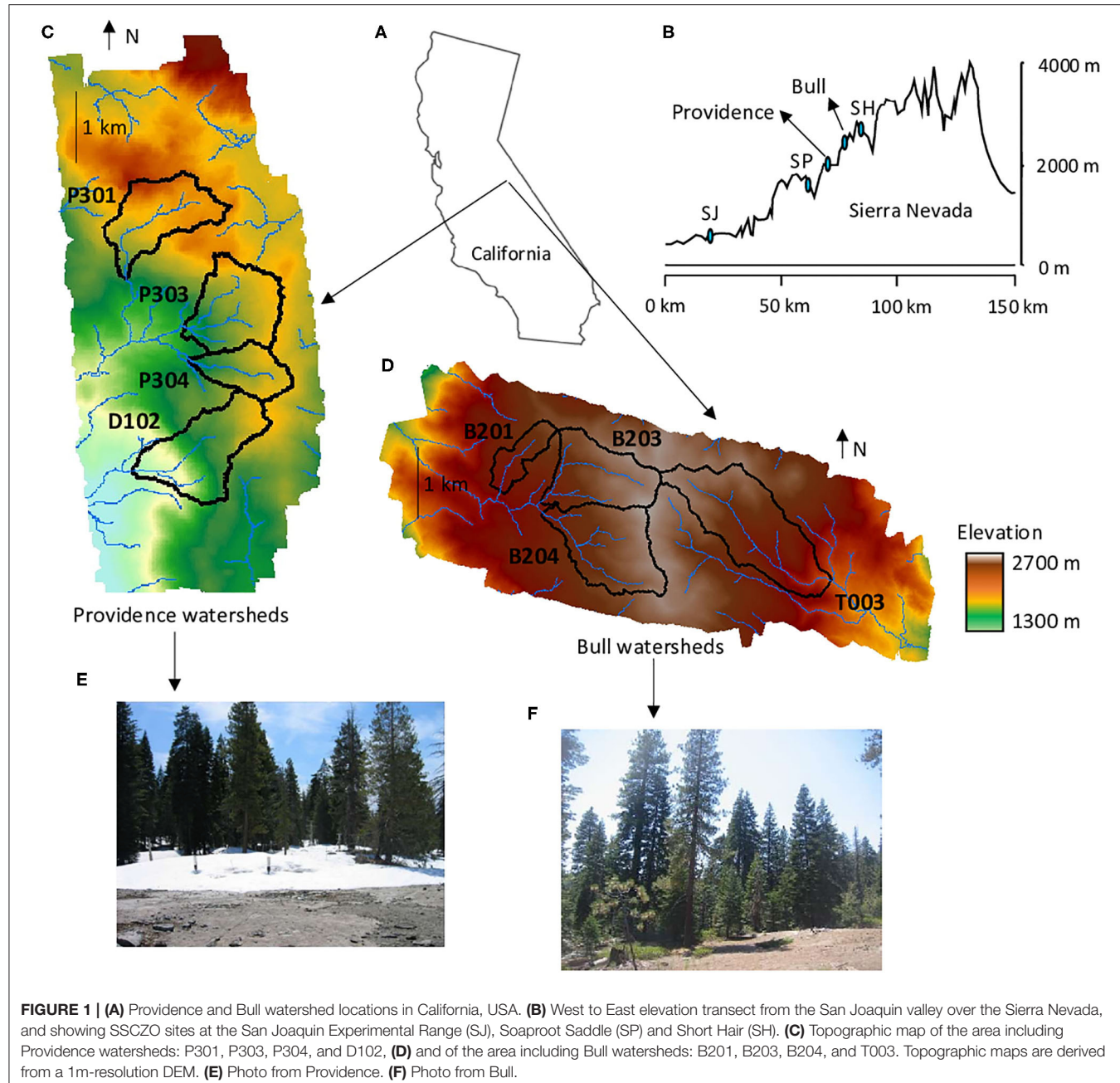
## METHODS

### Watershed Study Areas

This study focused on the Kings River Experimental Watersheds (KREW), an elevation gradient of watersheds characterized by different climates and geomorphologic features in the southern Sierra Nevada in California ( $37.068^{\circ}\text{N}$ ,  $119.191^{\circ}\text{W}$ ; Goulden et al., 2012; Liu et al., 2013; Holbrook et al., 2014; Safeeq and Hunsaker, 2016; Hunsaker and Johnson, 2017; Bales et al., 2018; O'Geen et al., 2018). KREW is a long-term and integrated project for CZ research and is operated by the U.S. Forest Service, Pacific Southwest Research Station.

KREW includes eight watersheds, four in Providence site (P301, P303, P304, and D102) and four in Bull site (B201, B203, B204, and T003; **Figure 1**). The study area is underlain by the Sierra Nevada Batholith with bedrock dominated by Mesozoic granitoids and metamorphic rocks from granitic roof pendants (Lackey et al., 2012; Callahan et al., 2019). The Landscape is characterized by a sequence of range-parallel ridges and valleys, with alternating steep and gentle terrain (Holbrook et al., 2014). Providence is located east of a tread edge in an area with generally intermediate slopes (Jessup et al., 2011). Bull is located southeast of Providence, with erosion and soil formation rates that are generally slower than Providence (Callahan et al., 2019). More geological description of the region and additional chemical and mineralogical data are available from the US Geological Survey (Bateman and Lockwood, 1976; Bateman and Busacca, 1983).

The climate is mountainous and Mediterranean with long dry summers and the majority of precipitation falling in winter. Providence watersheds have mean elevations between 1782 and 1979 m (**Figure 1**), a mean annual temperature around  $8^{\circ}\text{C}$  and a mean annual precipitation of approximately  $1015\text{ mm.yr}^{-1}$  (Safeeq and Hunsaker, 2016). The Providence group is located near the rain-snow transition zone (30–60% snow). Bull watersheds have mean elevations ranging from 2122 to 2373 m, a mean annual temperature around  $7^{\circ}\text{C}$  and a mean annual precipitation of approximately  $1386\text{ mm.yr}^{-1}$ . Most of the winter precipitation falls as snow in the Bull watersheds (70–90%; Hunsaker and Johnson, 2017). Soils are relatively shallow ( $<1\text{ m}$ ) Shaver and Cagwin soils and are all derived from granite



(Johnson et al., 2011). Vegetation in Providence is dominated by Sierran mixed-conifer forest with some mixed chaparral and barren land cover (Bales et al., 2011; Safeeq and Hunsaker, 2016). Vegetation in Bull is predominately red fir forest with some mixed-conifer forest at lower elevations.

## Data

This study is based on the long-term monitoring of the KREW and on the database from the Southern Sierra Critical Zone Observatory (SSCZO, Liu et al., 2013; Holbrook et al., 2014; Safeeq and Hunsaker, 2016; Hunsaker and Johnson, 2017; Bales

et al., 2018). Recent efforts have been undertaken to characterize the CZ structure and regolith properties along the SSCZO elevation gradient (O'Geen et al., 2018; Tian et al., 2019).

A drilling campaign involving Geoprobe sampling was organized to better estimate the regolith thickness and its variability across the SSCZO (O'Geen et al., 2018). Measured regolith thicknesses indicated thin regolith (1–2 m) at low elevation (400 m, SJ site, **Figure 1B**) and at high elevation (2,700 m, SH site, **Figure 1B**). From 1,100 to 2,000 m, measured thicknesses were higher but tended to decrease with elevation, with mean values around 5–6 m at 1,100 m and around 2–3 m

at 2,000 m (O'Geen et al., 2018). For the Providence and Bull watersheds (**Figure 1B**), regolith thickness was investigated in P301, P303, and D102 (1,700–2,000 m, 49 sampled sites), with mean thicknesses around 4–6 m.

Regolith density and porosity were estimated at several sites on samples collected during the Geoprobe campaigns (O'Geen

et al., 2018). Mean regolith density was approximately 1.5–1.7 g.cm<sup>-3</sup> and mean regolith porosity was approximately 0.35–0.40 between 0 and 6 m of depth. Hydraulic conductivities at saturation ( $K_{sat}$ ) were also measured on Geoprobe samples collected by O'Geen et al. (2018), and ranged from 0 to  $7 \times 10^{-5}$  m.s<sup>-1</sup>.  $K_{sat}$  values were high for a few points near the surface

**TABLE 1 |** Geochemical and mineralogical data for the regolith of the KREW.

| Oxide concentration <sup>a</sup> | CaO    | Na <sub>2</sub> O | MgO        | K <sub>2</sub> O | SiO <sub>2</sub> | Al <sub>2</sub> O <sub>3</sub> | Fe <sub>2</sub> O <sub>3</sub> |
|----------------------------------|--------|-------------------|------------|------------------|------------------|--------------------------------|--------------------------------|
| Providence                       | 4.35   | 2.52              | 2.56       | 2.42             | 62.45            | 17.75                          | 6.37                           |
| Bull                             | 0.56   | 0.91              | 0.59       | 2.66             | 81.25            | 10.58                          | 2.66                           |
| Mass fraction <sup>b</sup>       | Quartz | Albite            | K-feldspar | Biotite          | Muscovite        | Anorthite                      | Apatite                        |
| Providence                       | 30     | 32                | 6          | 15               | 6                | 10.5                           | 0.5                            |
| Bull                             | 52     | 19                | 9          | 10               | 4.5              | 5.3                            | 0.2                            |
| Reactive surface <sup>c</sup>    | Quartz | Albite            | K-feldspar | Biotite          | Muscovite        | Anorthite                      | Apatite                        |
| Providence                       | 15.5   | 3.2               | 0.7        | 3                | 0.6              | 3.2                            | 0.005                          |
| Bull                             | 23.3   | 1.9               | 0.9        | 2                | 0.5              | 1.6                            | 0.002                          |

<sup>a</sup>Data presented are mean values from all the regolith samples collected in Providence and Bull watersheds. Regolith samples were collected from top soil to the bottom of regolith by soil pit, hand auger or geoprobe sampling campaigns. Concentrations have been determined by ICP-AES and are expressed in % of mass of oxides. Analytical uncertainties are 5% for concentrations.

<sup>b</sup>Mineral mass fractions have been determined by XRD analysis and are expressed in %. Analytical uncertainties are 10 % for mineral mass fractions.

<sup>c</sup>Geometric surfaces are used as reactive surfaces for reactive-transport modeling. Reactive surfaces are expressed in m<sup>2</sup>.kg H<sub>2</sub>O<sup>-1</sup>.

**TABLE 2 |** Main geomorphologic features and stream water chemistry data.

|   | Providence watersheds |        |        |        | Bull watersheds |        |        |        |
|---|-----------------------|--------|--------|--------|-----------------|--------|--------|--------|
|   | P301                  | P303   | P304   | D102   | B201            | B203   | B204   | T003   |
| <b>GEOMORPHOLOGIC FEATURES<sup>a</sup></b>                  |                       |        |        |        |                 |        |        |        |
| Area, km <sup>2</sup>                                       | 0.97                  | 1.04   | 0.55   | 1.17   | 0.46            | 1.40   | 1.65   | 2.29   |
| Mean elevation, m   | 1979                  | 1905   | 1899   | 1782   | 2257            | 2373   | 2365   | 2289   |
| Mean slope, %   | 19                    | 20     | 22     | 27     | 18              | 18     | 17     | 24     |
| Relief, m   | 318                   | 292    | 213    | 491    | 225             | 303    | 289    | 414    |
| % of channel in meadows                                     | 16.4                  | 0      | 8.9    | 2.5    | 92              | 28.6   | 61.7   | 22.9   |
| Number of subsurface flow line                              | 42                    | 46     | 30     | 49     | 17              | 62     | 59     | 56     |
| Cumulative subsurface flow line length, km                  | 7.16                  | 8.75   | 3.72   | 12.18  | 3.02            | 10.59  | 10.57  | 11.48  |
| Mean subsurface flow line length, m                         | 200                   | 244    | 121    | 346    | 130             | 148    | 211    | 225    |
| Standard deviation of flow line length, m                   | 140                   | 233    | 90     | 225    | 90              | 83     | 185    | 213    |
| Cumulative stream network length, km                        | 2.40                  | 3.12   | 1.34   | 2.15   | 1.10            | 4.07   | 4.31   | 4.23   |
| <b>STREAM WATER<sup>b</sup></b>                             |                       |        |        |        |                 |        |        |        |
| Base flow index, BFI, %                                     | 71.6                  | 74.3   | 88.1   | 76.0   | 73.3            | 68.2   | 68.1   | 76.1   |
| Mean annual water discharge, L.s <sup>-1</sup>              | 34.1                  | 45.5   | 13.7   | 32.6   | 23.3            | 83.1   | 74.2   | 82.6   |
| Standard deviation of water discharge, L.s <sup>-1</sup>    | 56.5                  | 77.5   | 15.6   | 47.1   | 34.5            | 117.9  | 114.1  | 107.4  |
| Mean Ca <sup>2+</sup> concentration, $\mu\text{mol.L}^{-1}$ | 214                   | 268    | 327    | 261    | 109             | 73     | 106    | 165    |
| Mean Na <sup>+</sup> concentration, $\mu\text{mol.L}^{-1}$  | 114                   | 132    | 161    | 171    | 56              | 45     | 55     | 70     |
| $a_{\text{Ca}^{2+}}$  | 277                   | 384    | 489    | 340    | 161             | 92     | 141    | 263    |
| $b_{\text{Ca}^{2+}}$  | -0.117                | -0.154 | -0.196 | -0.110 | -0.195          | -0.080 | -0.095 | -0.135 |

<sup>a</sup>Geomorphologic features were determined using a 1-m resolution DEM and ArcGIS. Cumulative subsurface-flow-line and river-network lengths are given for average hydrologic conditions. BFI are from Safeeq and Hunsaker (2016).

<sup>b</sup>Stream chemistry data are from the 2003–2007 monitoring campaigns presented in Liu et al. (2013). The complete hydrogeochemical data are provided in Supplementary Material (**Table SM1**). The coefficients  $a_{\text{Ca}^{2+}}$  and  $b_{\text{Ca}^{2+}}$  were obtained by fitting a power law  $C = aQ^b$  along the C-Q relations from the KREW stream waters (**Figure 3**).

( $7 \times 10^{-5} \text{ m.s}^{-1}$ ), but much lower over the rest of the regolith column ( $0.8 \times 10^{-6} \text{ m.s}^{-1}$ ). The mean value of  $K_{\text{sat}}$  was  $6 \times 10^{-6} \text{ m.s}^{-1}$  for the entire regolith column.

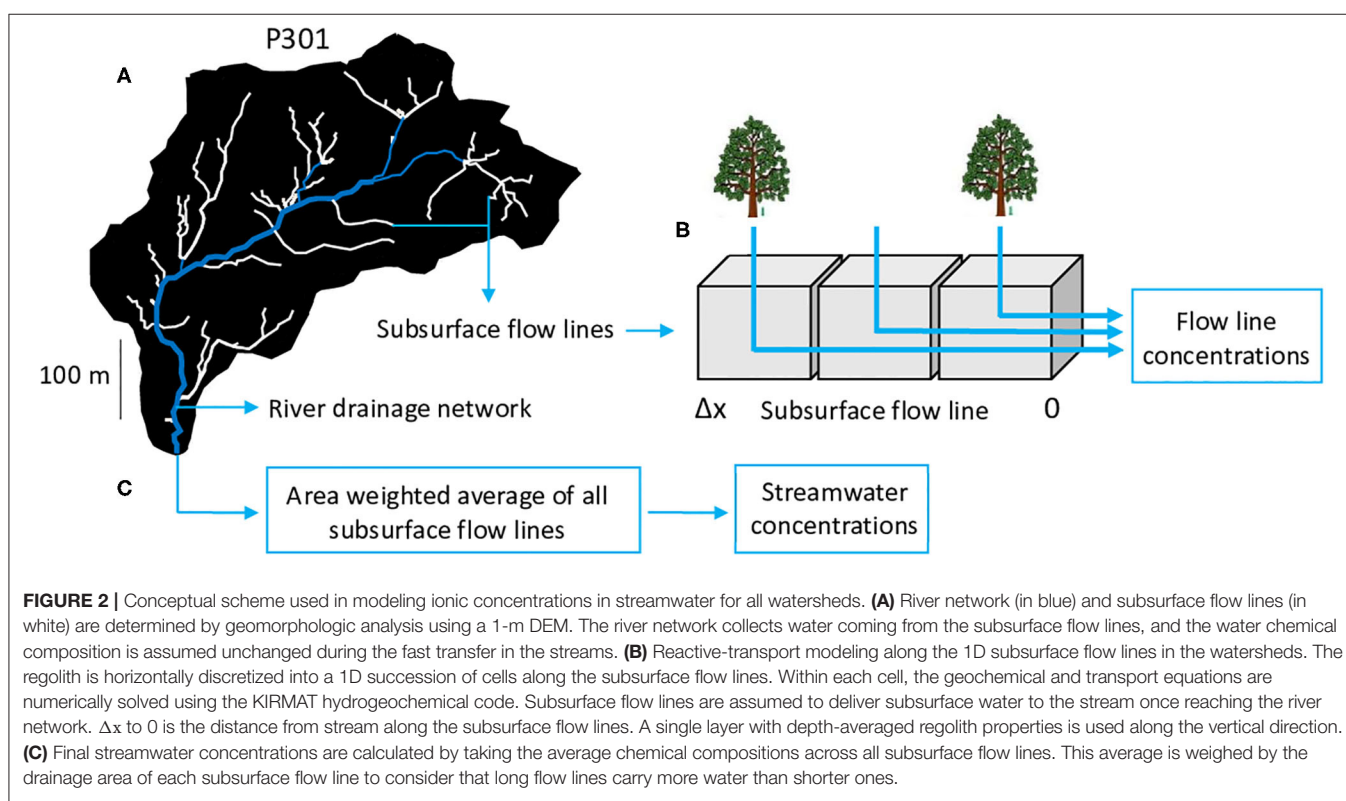
Soil and regolith samples were also collected in the KREW for geochemical and mineralogical analysis from soil-pit, hand-auger and/or Geoprobe campaigns (Johnson et al., 2011; O'Geen et al., 2018; Tian et al., 2019). Sampling depth was between 0 and 2 m, with a few samples from Geoprobe campaigns reaching 10 m in Providence. Mineralogical composition of regolith samples was determined by the quantitative interpretation of X-ray analysis reported by Tian et al. (2019), following Ackerer et al. (2016). Elemental concentrations in bulk regolith samples were also determined by ICP-AES following Tian et al. (2019). Regolith geochemistry and mineralogy were significantly different between Providence and Bull. The granite from Providence showed higher contents of Biotite, Anorthite, Albite and higher concentrations of Ca and Mg compared to Bull (Table 1). Bull bedrock is a quartz-rich granite with higher concentrations of SiO<sub>2</sub> but lower concentrations of Ca and Mg than Providence. Abundances of K-feldspar (6–9%) and concentrations of K (2.42–2.66%) were much more similar in the regolith of Providence and Bull watersheds (Table 1).

The SSCZO database on regolith geochemistry and mineralogy is supplemented by the hydrologic and geochemical monitoring of stream waters in the KREW (Liu et al., 2013; Safeeq and Hunsaker, 2016; Hunsaker and Johnson, 2017). Water discharge, pH, specific conductivity and solute concentrations of Na<sup>+</sup>, Ca<sup>2+</sup>, K<sup>+</sup>, and Mg<sup>2+</sup> were reported for the stream water at the KREW outlets for 2003–2007 (Liu et al., 2013). Mean annual

water discharge, standard deviation of water discharge, and mean annual concentrations of Ca<sup>2+</sup> and Na<sup>+</sup> are given in Table 2. The complete database for stream chemistry over the 2003–2007 period is available in Supplementary Materials (Table SM1). The hydroclimatic characteristics and other hydrologic signatures (e.g., base flow index) of the KREW have been reported by Safeeq and Hunsaker (2016).

## Geomorphologic Features

A 1-m resolution digital elevation model (DEM) derived from a recent airborne Lidar survey was analyzed to better constrain the geomorphologic features of all watersheds (Figure 1). Watershed areas, elevations, slopes and reliefs were calculated (Table 2). Accumulated flow from up-slope contributing areas to each cell of the DEM was determined (ArcGIS) to map the hydrologic drainage networks (Storck et al., 1998; Liu et al., 2003). A flow-accumulation threshold of 2,000 m<sup>2</sup> was selected to capture the main hydrologic drainage network along slopes, and the same threshold was used to highlight the inter-watershed differences. Comparison with the topographic maps from the U.S. Geological Survey and with field observations was performed to evaluate the hydrologic drainage networks and to distinguish streams and subsurface drainage networks. The stream networks represent observed channelized streams that are directly connected with the watershed outlets. The subsurface drainage networks represent the hydrologic drainage along the slopes, following the main topographic depressions, but where streams are not observed. Subsurface drainage networks connect with stream networks on the valley floors.



## C-Q Relations

C-Q relations were studied at the outlet of the KREW on the basis of the hydrologic and geochemical database of stream waters. Concentration-discharge relations were interpreted by fitting power laws of type  $C = aQ^b$  (e.g., Godsey et al., 2009; Chorover et al., 2017; Kim et al., 2017; Liu et al., 2017), with  $C$  the solute concentrations in stream waters ( $\mu\text{mol.L}^{-1}$ ) and  $Q$  the stream discharges at watershed outlets ( $\text{L.s}^{-1}$ ). Linear scales were preferred to better visualize the contrasting behavior of watersheds during dry periods. The  $a$  coefficient of the power law  $C = aQ^b$  controls the height of the C-Q relation (y-intercept, the constant in the power law equation), and has a strong correlation with the mean annual concentrations of stream waters. The  $b$  coefficient controls the curvature of the C-Q relation (the exponent in the power law equation), and is an indicator of the degree of chemodynamic behavior of stream waters. We used the threshold  $b = -0.1$  to distinguish chemostatic ( $0 > b > -0.1$ ) and chemodynamic watersheds ( $-0.1 > b$ ) as in Herndon et al. (2015) and Hunsaker and Johnson (2017).

To highlight the control of CZ structure on C-Q relations, we recommend working with a lithogenic solute sensitive to transit time variations along the subsurface flow lines: a solute with a strong Concentration-Mean Transit Time slope (C-MTT slope, Ackerer et al., 2020). The C-MTT slope considers the competition between primary mineral dissolution and incorporation into clay minerals, and indicates how fast a solute concentration rises with an increase of water transit time. A strong C-MTT slope facilitates the expression of CZ structure (e.g., length of subsurface flow paths, topography, watershed structure) on water chemical composition because stream water concentrations will be sensitive to physical attributes controlling water circulations in the watershed. In contrast, a solute with a low C-MTT slope may have stream water concentrations that are weakly responsive to the seasonal variability of transit times. In granitic watersheds,  $\text{Ca}^{2+}$  and  $\text{H}_4\text{SiO}_4$  typically have strong C-MTT slopes, while  $\text{K}^+$  and  $\text{Mg}^{2+}$  frequently show lower C-MTT slopes (Ackerer et al., 2020). We focused in this study on the detailed understanding of C-Q relations for  $\text{Ca}^{2+}$  as this ion has an extensive database, a strong C-MTT slope, and shows the most contrast in C-Q relations across the KREW. The  $a$  and  $b$  coefficients for  $\text{Ca}^{2+}$  are written  $a_{\text{Ca}^{2+}}$  and  $b_{\text{Ca}^{2+}}$  in the following sections.

## The KIRMAT Reactive-Transport Code

Hydrogeochemical simulations were performed with the 1D thermo-kinetic code KIRMAT (KInetic of Reaction and MAss Transport; Gérard et al., 1998; Ngo et al., 2014; Lucas et al., 2017; Ackerer et al., 2018). KIRMAT is based on the Transition State Theory (TST) and solves the equations describing geochemical reactions and transport mass balance in a porous medium. Transport processes include the effects of convection, diffusion and kinematic dispersion. Chemical reactions account for the dissolution of primary minerals, oxido-reduction reactions, and the formation of secondary minerals and clay minerals. The clay fraction is defined in KIRMAT as a solid solution made up of a combination of pure clay end-members (Tardy and Fritz, 1981). The clay solid solution is precipitated at thermodynamic equilibrium and its composition varies over time depending on the water chemistry and the evolution of regolith mineralogy (Ackerer et al., 2018). The KIRMAT code also considers feedback effects between mineral mass budgets, reactive surfaces, and changes in bedrock porosity (Ngo et al., 2014). The framework of geochemical modeling with KIRMAT in granitic watersheds is available in Ackerer et al. (2018, 2020). More specific data on the geochemical modeling, kinetic and thermodynamic constants are available in **Tables SM2–SM5**.

## Hydrogeochemical Modeling Strategy

The modeling strategy to consider the variability of the CZ structure over the KREW is adapted from Ackerer et al. (2018, 2020). Reactive-transport modeling was first performed on P301, as this reference watershed has the most extensive database and a high density of regolith-thickness measurements. Regolith mineralogy and geochemistry were constrained in P301 by the mineralogical and geochemical analysis (**Table 1**). Simple geometric surfaces are used as reactive surfaces for the dissolution reactions of primary minerals (**Table 1**). Estimates from Geoprobe campaigns of mean porosity (0.35) and mean hydraulic conductivity ( $6 \times 10^{-6} \text{ m.s}^{-1}$ ) along the regolith column were used for all simulations. Slopes are known from the DEM, and the C-Q relations at the P301 outlet were constrained by the hydrochemical database (**Table 2**, **Table SM1**). Average saturated zone thickness is unknown over P301 but measurements of regolith thickness provide a maximum value.

**TABLE 3 |** Modeling results for the eight watersheds.

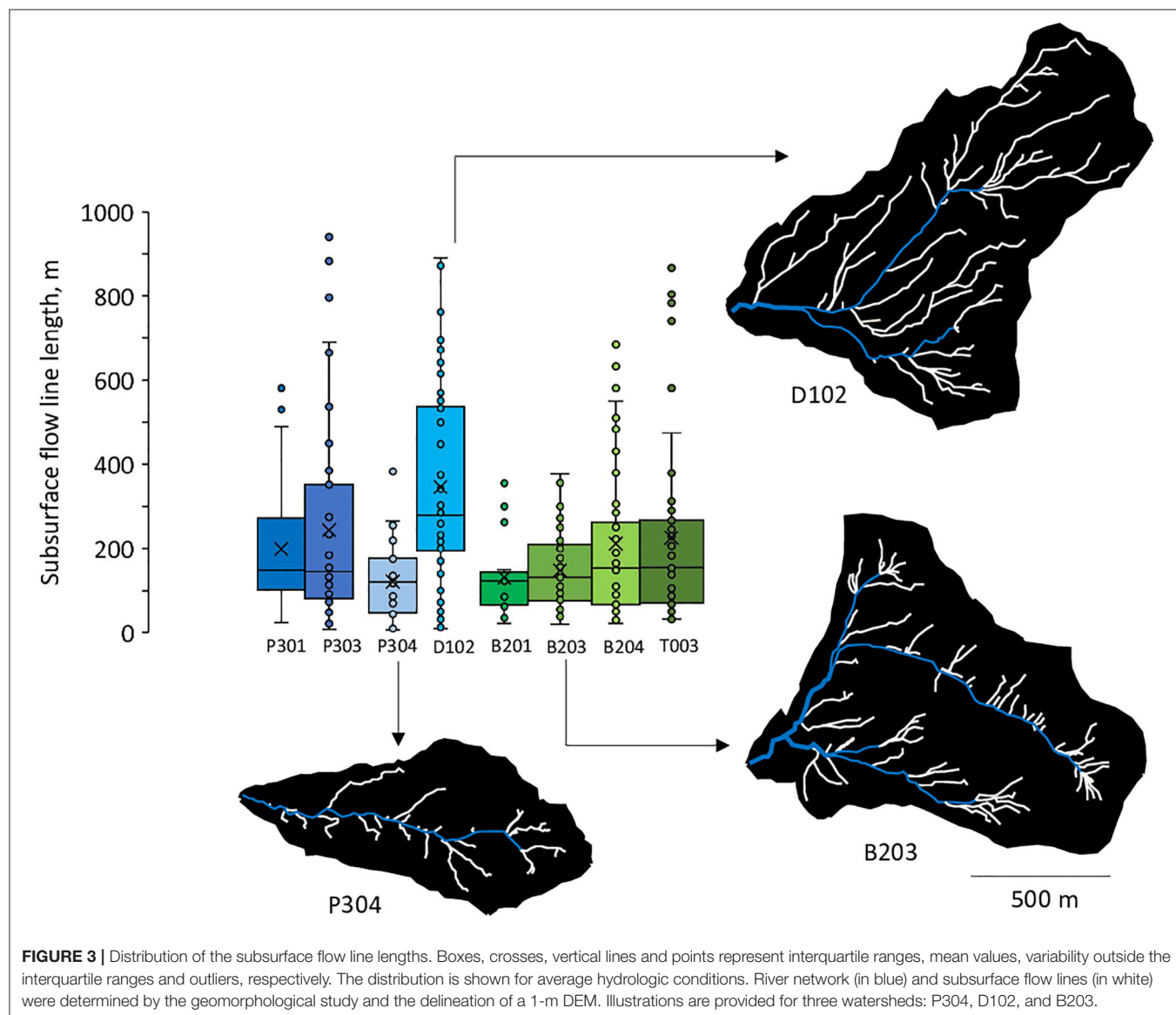
|   | Providence |      |      |      | Bull |      |      |      |
|---|------------|------|------|------|------|------|------|------|
|   | P301       | P303 | P304 | D102 | B201 | B203 | B204 | T003 |
| <b>MODELING RESULTS<sup>a</sup></b>               |            |      |      |      |      |      |      |      |
| Saturated thickness, m                            | 4          | 4.5  | 7    | 4.5  | 6    | 3    | 3    | 4    |
| RMSE (%)  | 6.5        | 8.0  | 4.9  | 7.2  | 5.4  | 12.8 | 11.2 | 9.1  |
| Mean subsurface flow velocity, $\text{m.yr}^{-1}$ | 53         | 53   | 19   | 76   | 27   | 70   | 63   | 39   |
| Mean stream water transit time, yr                | 4.1        | 5.7  | 7.6  | 5.1  | 4.9  | 2.8  | 3.5  | 6.5  |

<sup>a</sup>Estimated saturated thicknesses are determined through hydrogeochemical modeling by fitting C-Q data. Root mean square errors are given for the fit of C-Q relations. Mean subsurface flow velocities are given for average hydrologic conditions and for simulations matching C-Q data. Mean subsurface water transit times are given for average hydrologic conditions and by combining subsurface flow line lengths and flow velocities.

A schematic view of the modeling strategy is presented for P301 in **Figure 2**. Modeling was performed for a selection of dates covering the entire range of hydrologic conditions, from summer and fall dry periods to winter and spring floods. Dates were selected on the basis of stream discharges at the outlets by selecting days corresponding to 1, 10, 35, 50, and 100% of the maximum observed stream discharge. The selection is biased toward lower discharges because chemical concentrations vary dramatically at lower discharges, which dictates the C-Q power-law curvature. A set of simulations was done for each date. Reactive-transport simulations were performed along the subsurface drainage network identified by the geomorphologic analysis. For a given date and along each subsurface flow line, a 1D simulation with KIRMAT was performed to constrain the evolution of the subsurface water chemistry (**Figure 2**). Soil solutions were used as input solutions percolating into the

regolith (**Figure 2B**, chemical data from Liu et al., 2013). Flow velocities along the subsurface flow lines were estimated using the ArcGIS groundwater toolset. Flow velocities were controlled by slopes, porosity, hydraulic conductivity and saturated thickness. These parameters were generated from the KREW database, except the saturated zone thicknesses, which was adjusted by a Monte-Carlo approach to obtain the best fit between modeled and measured C-Q relations at the P301 outlet. The fits were quantified using the root mean square error (RMSE, **Table 3**) and the mean value of regolith thickness on P301 was used as a maximum boundary.

The modeled C-Q relations were determined as follows. The simulated concentrations in the stream at a watershed's outlet were calculated by taking the landscape surface-area-weighted average of concentrations from all the subsurface flow lines (**Figure 2**). The simulated stream discharge was calculated by



summing the water discharges over all the subsurface flow lines. This sum was also landscape surface-area weighted to consider that longer subsurface flow lines draining large areas carry more water than shorter flow lines. Water transit times were calculated along each subsurface flow line by combining lengths of subsurface flow lines and subsurface flow velocities. The mean transit time for stream water was determined by taking the surface-area-weighted average of transit times from all subsurface flow lines.

Our depth-integrated, reactive-transport modeling was performed within a single regolith layer with averaged mineralogical, geochemical and physical properties. It is assumed that the subsurface waters are delivered to stream once the subsurface flow lines reach the stream network. Chemical composition of stream water is also assumed to remain unchanged during the fast transfer within the stream network. This assumption is supported by the short length of the stream network in this type of headwater watersheds ( $<1$  km).

After the P301 watershed, this modeling strategy was extended to other seven watersheds. Differences in regolith mineralogy and chemical composition were considered for

the Providence and the Bull groups (Table 1). Modeling also considers the variability of the geomorphic features between the watersheds (Table 2). Regolith porosity and hydraulic conductivity measured in P301 were used for all the other watersheds. Modeled stream water concentrations and stream discharges were compared to measured values. The modeling of C-Q relations was used to estimate the saturated thicknesses over the watersheds where data on stream water and regolith are available but where regolith thicknesses are unknown (Table 3).

## RESULTS

### Variability of CZ Structure

The watersheds show contrasting CZ structures and subsurface-flow line distributions along the elevation gradient (Figure 3 and Table 2, Figure SM1 in Supplementary Materials). P304 and B201 are the smallest watersheds ( $0.5\text{ km}^2$ ), with limited stream networks (1.2 km), and a limited number of subsurface flow lines (20) characterized by compact length distributions around low values. T003 and B204 are the largest watersheds ( $2\text{ km}^2$ ), with the longest stream networks (4.2 km), and a high number of subsurface flow lines (60) characterized by relatively scattered length distributions around intermediate values. P301, P303, and D102 are intermediate size watersheds ( $1\text{ km}^2$ ), with intermediate stream networks (2.5 km), and a moderate number of subsurface flow lines (40). The standard deviation of the subsurface-flow-line lengths increases from P301 to P303 and D102. B203 is a relatively large watershed ( $1.7\text{ km}^2$ ), with a large stream network (4 km), but a high number of subsurface flow lines (60) characterized by a compact length distribution around short value. These contrasting CZ structures imply different degrees of connectivity between the subsurface drainage networks and streams.

### Hydrology and C-Q Relations

The watersheds are characterized by distinctive hydrogeochemical behaviors. Mean annual stream discharges are generally higher at Bull (B203, B204, T003), but stream discharges in these watersheds also show a higher annual variability with higher standard deviations (Table 2). B201 is an exception in the Bull group, with lower mean discharge and standard deviation. Providence watersheds have relatively low mean annual stream discharges, with P304 having the lowest discharge and standard deviation (Table 2). These trends in stream discharge are consistent with the base flow index (BFI) calculated over the KREW watersheds by Safeeq and Hunsaker (2016). The BFI is low for watersheds with a greater variability of discharge (B203, B204) and high for the watersheds with low and less variable discharges (B201, P304; Table 2).

Mean annual  $\text{Ca}^{2+}$  concentrations in stream water are lower in Bull compared to Providence watersheds (Table 2 and Figure 4A). The mean ionic concentrations in stream waters in Providence and Bull span the range between those of snowmelt and deep groundwater (Figure 4A). The mean concentrations in soil water are outside of this trend. Concentrations in stream water also vary seasonally, as illustrated by  $\text{Ca}^{2+}$  concentrations on Figure 4B. Periods of higher discharge during winter and

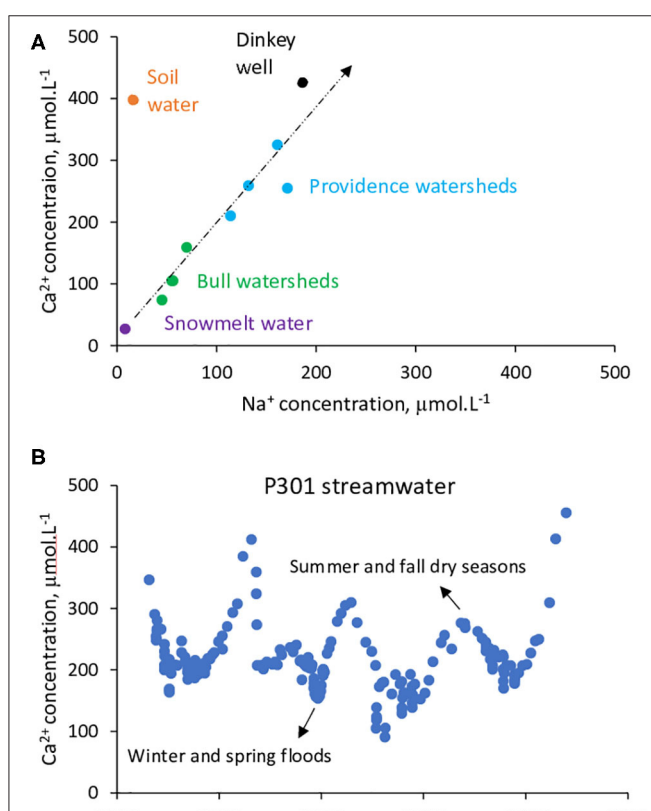


**FIGURE 4 |** Overview of the chemical variability for Providence and Bull stream waters. **(A)** Elemental  $\text{Na}^{+}$  –  $\text{Ca}^{2+}$  diagram with mean annual solute concentrations for Providence and Bull stream waters, snowmelt, soil water and Dinkey well groundwater (4 km from Providence). Data from Liu et al. (2013). **(B)** Seasonal variability of  $\text{Ca}^{2+}$  concentrations for P301 streamwaters. Data are shown for period studied (2003–2007).

spring are typically characterized by lower concentrations, while values during summer and fall being frequently higher. The interannual variability of stream concentrations mainly follows climatic patterns, with higher concentrations in dry years and lower ones in wet years.

The diversity of CZ structures produces contrasting C-Q relations along the elevation gradient (**Figure 5** and **Figure SM4**). B203 and B204 show low  $a$  coefficient and chemostatic behavior ( $a_{Ca^{2+}} = 92$  to 141,  $0 > b_{Ca^{2+}} > -0.1$  with  $b_{Ca^{2+}} = -0.080$  to  $-0.095$ ) (**Figures 5E,G**). P301, P303, D102, and T003 show

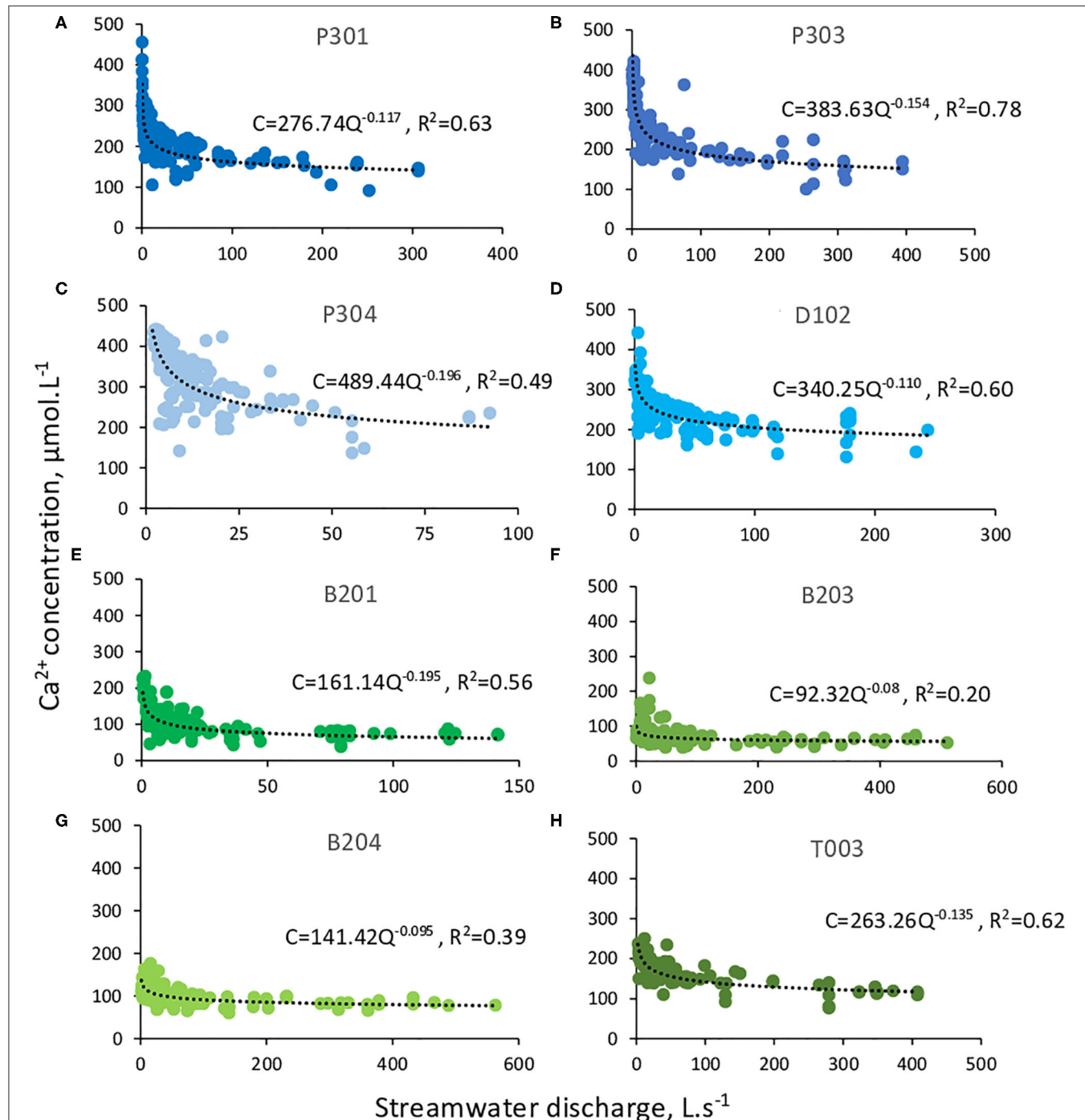


**FIGURE 5 | (A–H)**  $\text{Ca}^{2+}$  concentration-discharge relations for the eight watersheds. Each point represents a stream water sample. Power laws were fitted by using the expression  $C = aQ^b$ , with  $C$  the solute concentration in  $\mu\text{mol.L}^{-1}$ ,  $Q$  the streamwater discharge in  $\text{L.s}^{-1}$ ,  $a$  the coefficient determining the height of the law and  $b$  the coefficient setting the curvature of the law.

intermediate  $a$  coefficient and slightly chemodynamic behavior ( $a_{Ca2+} = 277$  to 384,  $-0.1 > b_{Ca2+} > -0.16$  with  $b_{Ca2+} = -0.110$  to  $-0.154$ ) (Figures 5A,B,D,H). B201 and P304 are the most chemodynamic watersheds ( $-0.1 > b_{Ca2+}$  with  $b_{Ca2+} = -0.195$  to  $-0.196$ ) (Figures 5C,E), but B201 displays low  $a$  coefficient ( $a_{Ca2+} = 161$ ), while P304 is characterized by high  $a$  coefficient ( $a_{Ca2+} = 489$ ). Two extreme end members can be identified. P304 is the most chemodynamic, with also the highest  $a$  coefficient ( $b_{Ca2+} = -0.196$ ,  $a_{Ca2+} = 489$ , Table 2 and Figure 5C). In contrast, B203 is the most chemostatic, with also the lowest  $a$  coefficient ( $b_{Ca2+} = -0.080$ ,  $a_{Ca2+} = 92$ , Table 2 and Figure 5F). The combination of chemostatic behavior with high mean concentration is not observed in any of the watersheds. Although a different threshold for distinguishing chemostatic and chemodynamic behavior ( $b_{Ca2+} = -0.1$ ) would slightly change the above classification, we highlight that we did not necessarily seek an absolute separation between watersheds classified as chemostatic or chemodynamic. Instead, our objective was to interpret the general trend of  $b_{Ca2+}$  and to propose a physical interpretation of this trend.

The  $a_{Ca2+}$  coefficient tends to decrease with increasing watershed elevation (Figure 6A), following the first-order difference of regolith geochemistry between the Providence and

Bull groups (Table 1). The  $a_{Ca2+}$  coefficient is also strongly correlated with the base flow index (BFI) calculated over the watersheds (Figure 6B). In Figure 6B, Providence and Bull groups are shifted, with higher  $a_{Ca2+}$  values for Providence, but within each group the  $a_{Ca2+}$  coefficient clearly increases with BFI. The  $b_{Ca2+}$  coefficient shows correlations with cumulative subsurface-flow-line length and to a lesser extent with mean annual stream discharge (Figures 6C,D). Watersheds with lower values of cumulative subsurface flow line length and with both lower annual mean discharge and discharge variability are the most chemodynamic (P304 and B201,  $b_{Ca2+} = -0.195$  to  $-0.196$ ). Watersheds with higher values of cumulative subsurface flow line length and with both higher annual mean discharge and discharge variability are more chemostatic (B203 and B204,  $b_{Ca2+} = -0.080$  to  $-0.095$ ). No correlations were found between stream discharge,  $a_{Ca2+}$ ,  $b_{Ca2+}$  and the meadow area (Table 2).

## Modeling Results for the Reference Watershed P301

The best agreement between measured and modeled C-Q relations for the reference watershed P301 was obtained with a mean saturated thickness of 4 m (Figure 7). With a 4-m thickness both discharge and  $\text{Ca}^{2+}$  concentrations were correctly

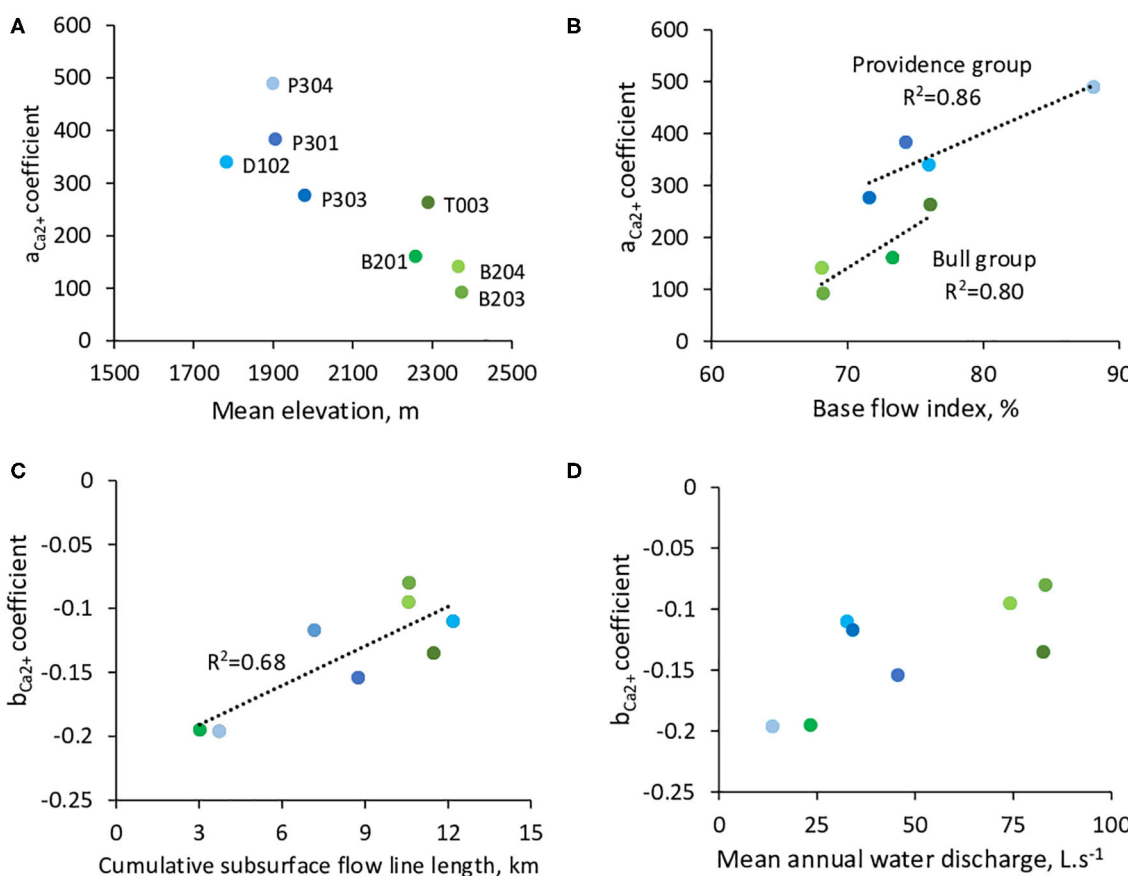
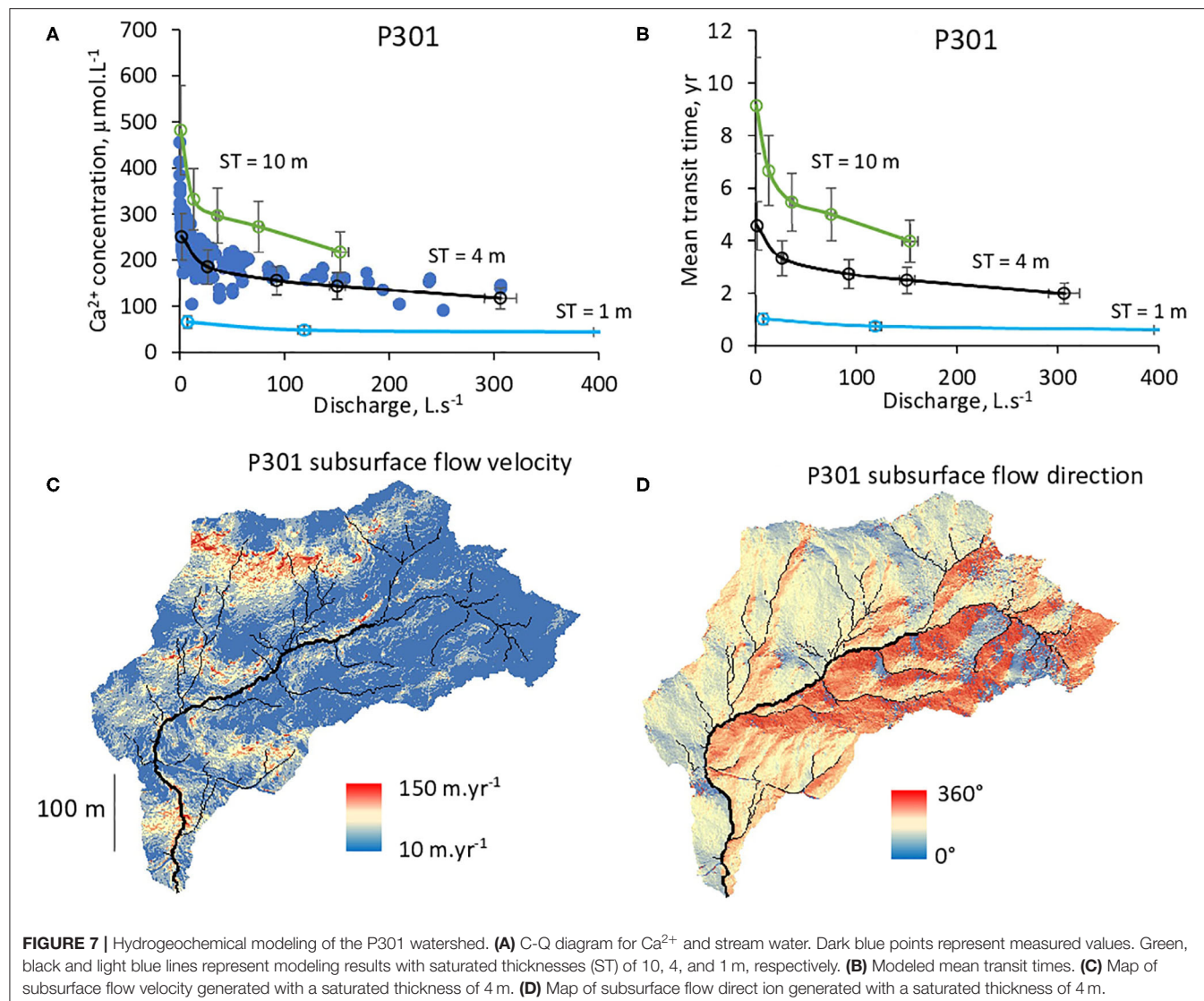


**FIGURE 6 |** Relations between C-Q shapes ( $a_{Ca2+}$  and  $b_{Ca2+}$  coefficients) and a selection of geomorphologic and hydrologic features for the KREW watersheds. **(A)**  $a_{Ca2+}$  vs. mean watershed elevations (m). **(B)** Relationship between  $a_{Ca2+}$  and the base flow index for the KREW watersheds. The values of base flow index are from Safeeq and Hunsaker (2016). **(C)**  $b_{Ca2+}$  vs. cumulative length of the subsurface flow lines. **(D)**  $b_{Ca2+}$  vs. mean annual water discharge from the streams at the outlets.



captured at the P301 outlet (Figure 7A). Simulations with a thinner or thicker mean saturated thicknesses underestimate or overpredict  $\text{Ca}^{2+}$  concentrations, respectively. For illustration, simulations with a mean saturated thickness of 1 m produced faster subsurface flows, shorter transit times and underestimated the  $\text{Ca}^{2+}$  concentrations at the outlet (Figures 7A,B). In contrast, simulations with a mean saturated thickness of 10 m generated slower flows and longer transit times, but overpredict stream water  $\text{Ca}^{2+}$  concentrations (Figures 7A,B).

For the best fit with a saturated thickness of 4 m, the simulated subsurface flow velocities vary between 10 and  $150 \text{ m.yr}^{-1}$  along the watershed's slopes (Figure 7C). Gentle parts (slope  $< 20\%$ ) of the watershed have slower velocities while faster subsurface flows take place in the steep (slope  $> 20\%$ ) northern parts (Figure 7C). The calculated mean transit times for the stream waters range between 2 year for the wettest conditions and 5 year for the driest periods observed between 2003 and 2007 (Figure 7B). The average mean transit time

over the 2003–2007 period for the P301 stream water is 4.1 year (Table 3).

## Modeling Results for All Watersheds

The estimated values of mean saturated thicknesses that best match the C-Q relations vary between 3 and 7 m (Table 3). The thinnest mean saturated thicknesses (ST) are located in the higher-elevation B203 and B204 watersheds (3 m). T003, D102, P301, and P303 have intermediate values (4–5 m). The largest estimates of mean saturated thickness are in B201 and P304 (6–7 m). Mean subsurface flow velocities are between 27 and  $76 \text{ m.yr}^{-1}$  (Table 3). Steep slopes (D102) and/or thin saturated thicknesses (B203) generate higher velocities (Figure 8), while watersheds with gentler slopes and thicker saturated thicknesses (B201, P304) have lower velocities (Figure 8, Figure SM2 in Supplementary Materials).

The contrasting CZ structures and subsurface-drainage networks imply different distributions of mean transit times

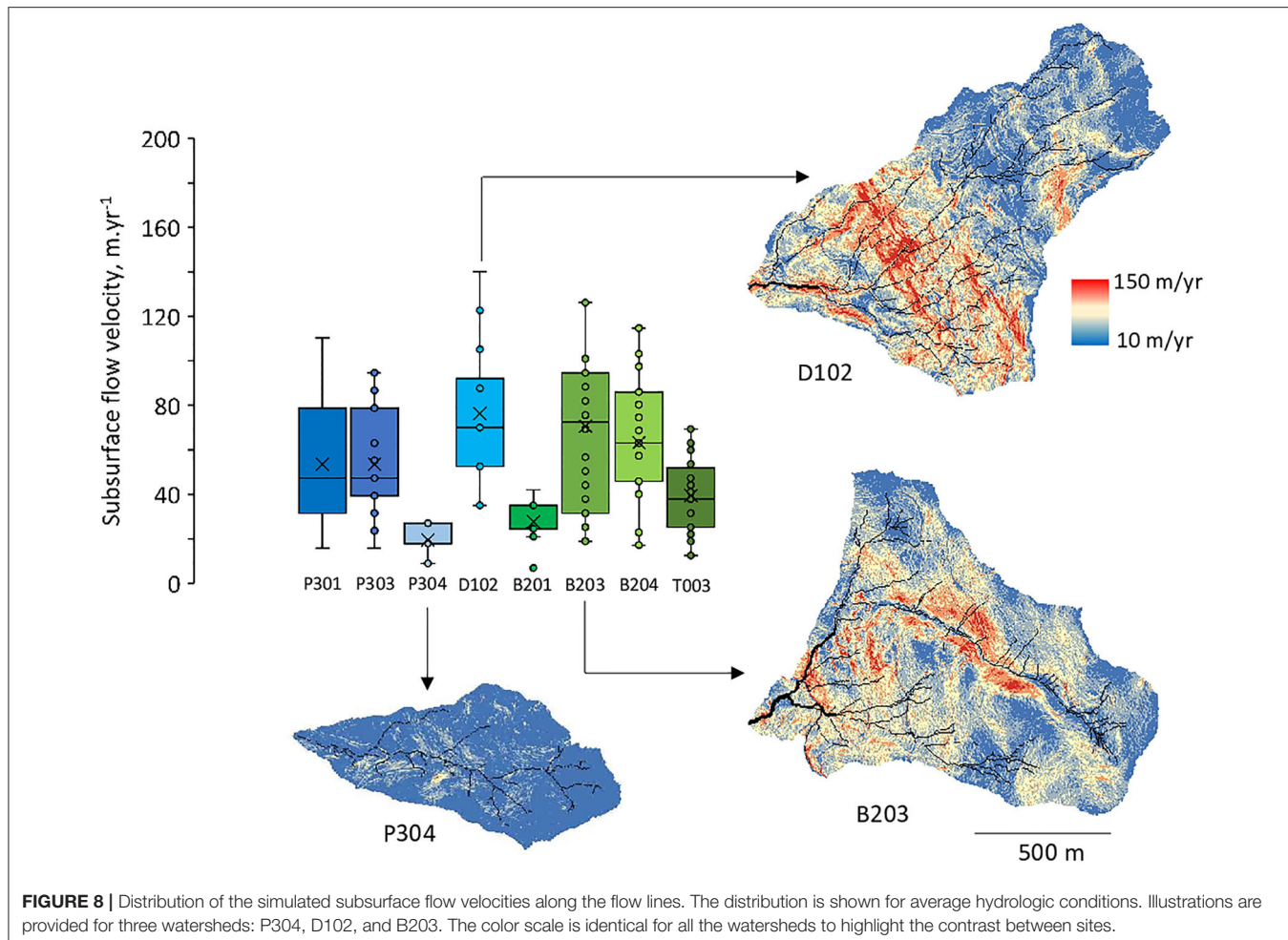


**FIGURE 8 |** Distribution of the simulated subsurface flow velocities along the flow lines. The distribution is shown for average hydrologic conditions. Illustrations are provided for three watersheds: P304, D102, and B203. The color scale is identical for all the watersheds to highlight the contrast between sites.

along the subsurface flow lines. Both velocities and flow line lengths control mean transit times. Shorter flow lines and faster velocities generate shorter transit times (**Figures 9, 10**, i.e. B203 and B204). Watersheds with longer subsurface flow lines and/or slower velocities tend to have longer transit times (**Figures 9, 10**, i.e., B201, T003 and P304, **Figure SM3** in Supplementary Materials). Estimated average mean transit times range from 2.8 year (B203) to 7.6 year (P304, **Table 3**). The simulated C-Q relations and mean transit times for all the KREW are given in **Figure 10**. Simulations capture the observed C-Q relations for the watersheds.

A strong negative correlation is observed between  $b_{Ca2+}$  and the estimated saturated thicknesses ( $R^2 = 0.86$ , **Figure 11A**). Watersheds with thin saturated thicknesses are the most chemostatic (B203 and B204, ST = 3 m,  $b_{Ca2+} = -0.080$  to  $-0.095$ ), while watersheds with thicker saturated thicknesses are more chemodynamic (B201 and P304, ST=6 to 7 m,  $b_{Ca2+} = -0.195$  to  $-0.196$ ). A good correlation is also found between the calculated mean transit times of stream water and BFI (**Figure 11B**). The watersheds with a higher proportion of base flows are consistently characterized by longer mean transit times.

## DISCUSSION

### Sensitivity Tests and Model Uncertainties

Multiple tests and simulations were performed to evaluate the sensitivity of the model to data uncertainties. This exercise allows to estimate how the uncertainties from regolith properties could impact model results and simulated C-Q relations. The first set of simulations was performed to estimate the impact of analytical uncertainties in regolith mineralogy on ionic concentrations in stream water. Increasing the mass fraction of Ca-bearing minerals by 10% while keeping other parameters constant increases the  $Ca^{2+}$  concentrations in P301 stream water by approximately 6%. The  $a_{Ca2+}$  coefficient of the simulated C-Q relation increases by 6%, while the  $b_{Ca2+}$  coefficient increases only by 1%. Thus, the simulated C-Q relation is affected by the mineralogical variations primarily through changes in the height of the C-Q relation ( $a_{Ca2+}$ ). Simulated mean transit times are not impacted by mineralogical variations.

We also tested the impact of uncertainties in soil-solution composition on simulated stream water concentrations. An increase of 1% of  $Ca^{2+}$  concentration in soil solutions has a negligible impact on mean  $Ca^{2+}$  concentrations in stream

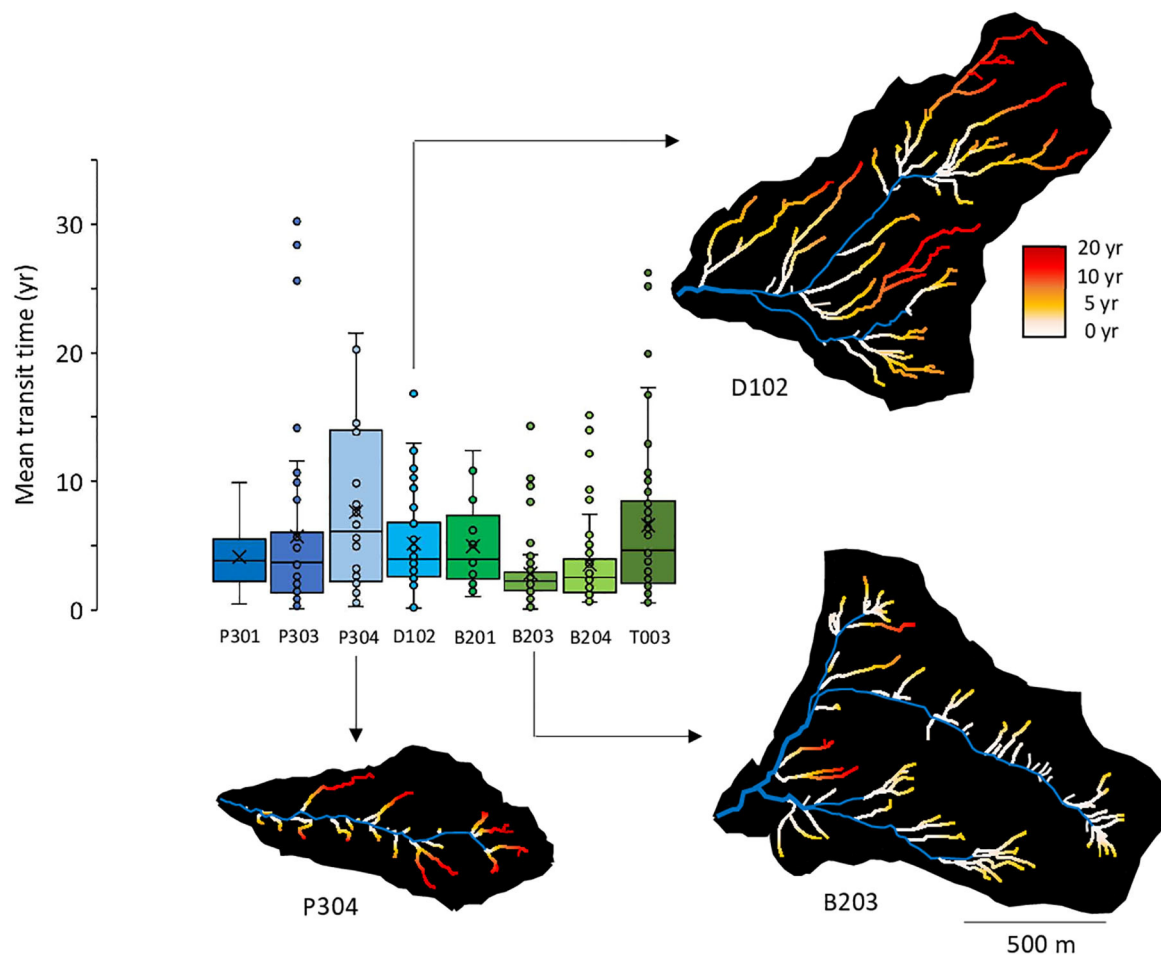


**FIGURE 9 |** Distribution of the simulated mean transit times along the subsurface flow lines. The distribution is shown for average hydrologic conditions. Mean transit times were calculated by combining subsurface flow line lengths and flow velocities. Illustrations are provided for three watersheds: P304, D102, and B203. The color scale is identical for all the watersheds to highlight the contrast between sites.

waters and  $a_{Ca2+}$  (variations of 0.5%). The coefficient  $b_{Ca2+}$  is insensitive to variations of soil solution concentrations. Variations of the soil solution pH from 6 to 6.5 modify  $a_{Ca2+}$  by 1–8 % but have no effects on  $b_{Ca2+}$ . The modeled chemodynamic behavior is therefore not very sensitive to chemical compositions of soil solutions used as input solutions into the regolith. Simulated mean transit times are not impacted by soil-solution variations.

The model sensitivity to variations of regolith porosity and hydraulic conductivity at saturation ( $K_{sat}$ ) has been also explored.  $a_{Ca2+}$  is affected by variations of porosity, with a 5–20% increase associated with 5–30% increase in porosity.  $b_{Ca2+}$  only weakly responds by 1–2%, and the mean transit times are not impacted by porosity variation alone. Our sensitivity analysis reveals that hydraulic conductivity is a key parameter for the modeling of C-Q relations. Both  $a_{Ca2+}$  and  $b_{Ca2+}$  are sensitive to modifications of  $K_{sat}$ . Increasing  $K_{sat}$  by 5–30% decreases  $a_{Ca2+}$  by 6–20% and decreases  $b_{Ca2+}$  by 3–6%. Mean transit times inferred from the modeling are also sensitive to  $K_{sat}$ , with

transit times decreasing by 5–30% when  $K_{sat}$  increases by 5–30%. Relying on field measurements of  $K_{sat}$  as well as porosity and regolith mineralogical characterization is therefore important for accurate modeling of C-Q relations.

### Comparison With Independent Estimates

Modeling results can be compared with independent estimates from field campaigns, geophysical sampling and results from isotopic studies. In a recent study, cosmogenic isotopes in stream water (tritium, sodium-22 and sulfur-35) were combined with the modeling of age-ranked storage selection to estimate water ages for the P301 stream (Visser et al., 2019). They found the mean age of stream water for 2004–2016 was 4.4 year. The value for 2003–2007 was 4.5 year, which was similar to the 4.1 year estimate of mean transit time our study computed from hydrogeochemical modeling over the same period (Table 3).

On the basis of age-ranked storage-selection modeling, Visser et al. (2019) also found that the regolith of P301 averaged 3 m of water in storage, varying between 2.7 m for dry years and

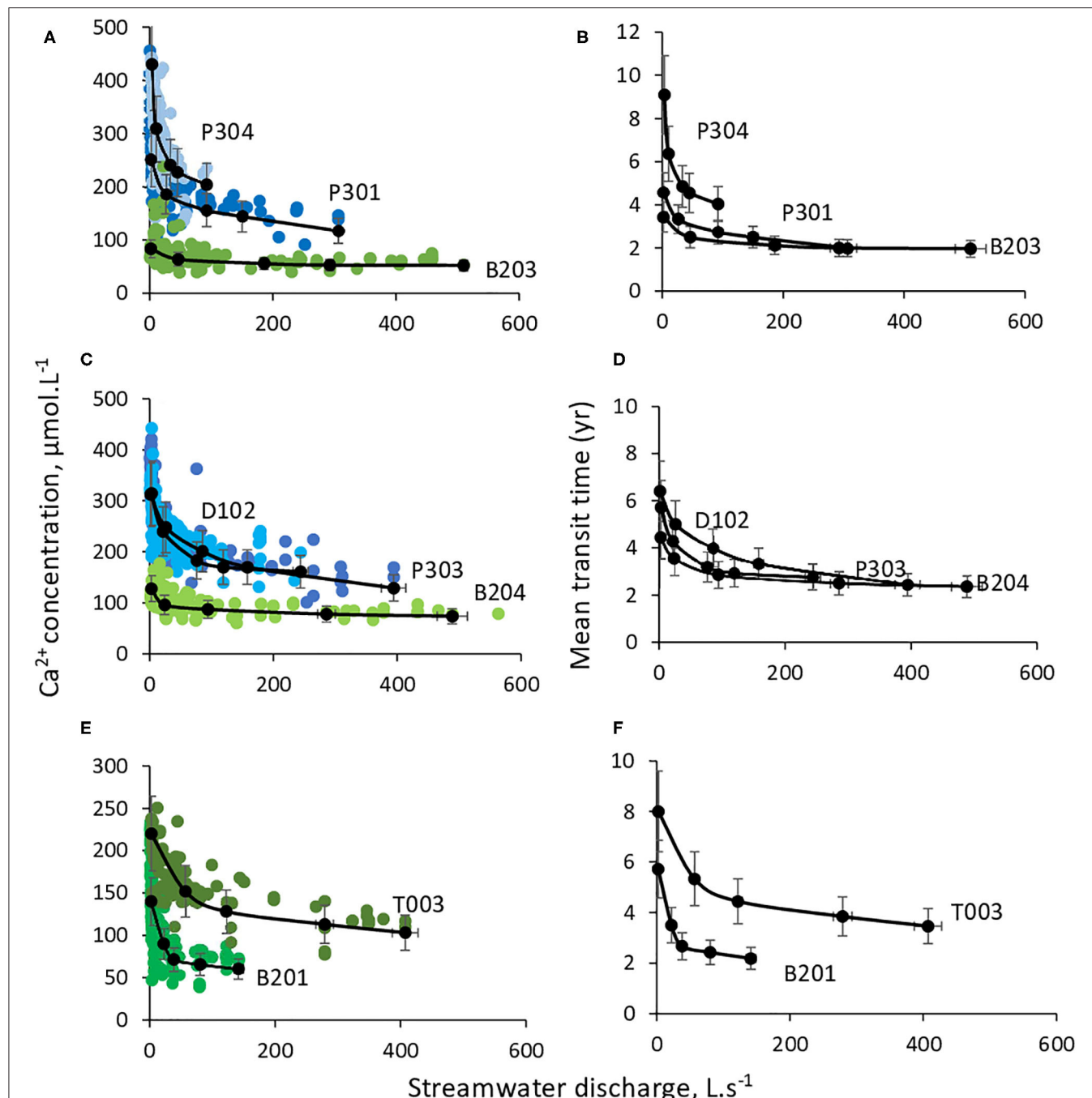
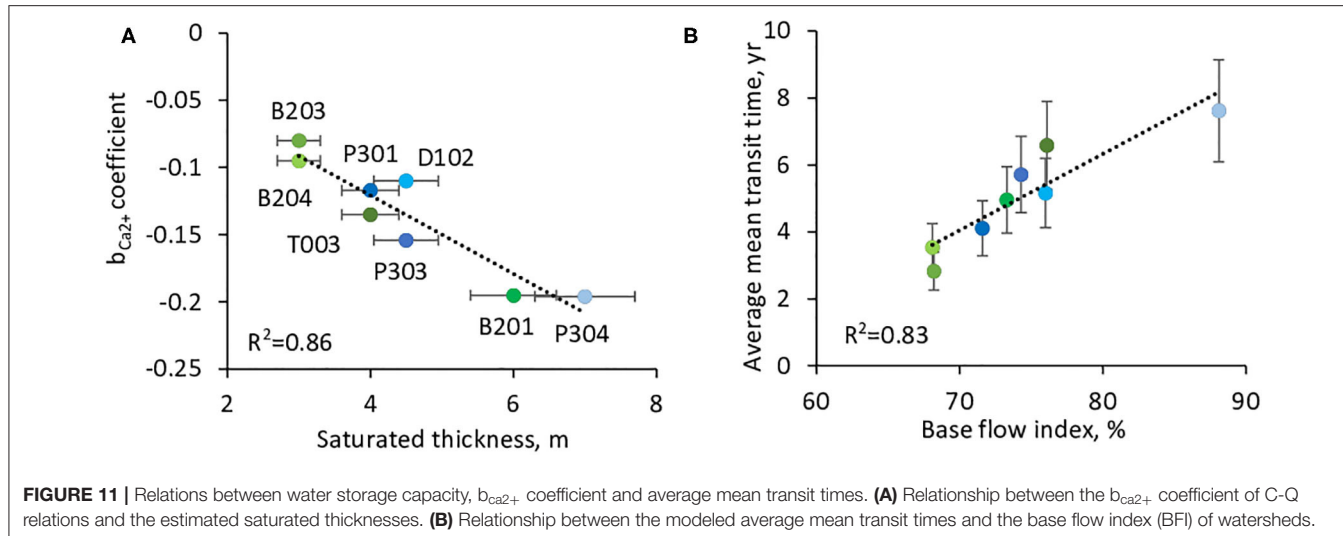


**FIGURE 10 |** Modeling results of C-Q relations (**A,C,E**) and mean transit times (**B,D,F**) for all the KREW stream waters. Black lines show modeling results and color points represent measured values.

4 m for wet years. Other geophysical investigations involving seismic refraction and tomographic inversion have estimated a water-storage potential between 1 and 5 m along P301 slopes, averaging 3 m for P301 (Holbrook et al., 2014). All of these mean values are similar to the average saturated thickness of 4 m inferred in P301 from our hydrogeochemical modeling of C-Q relations.

The estimates of mean saturated thicknesses obtained from hydrogeochemical modeling can be compared with the regolith thicknesses that have been measured from Geoprobe sampling in Providence (O'Geen et al., 2018). The mean saturated thicknesses must be equal or less than the average regolith thicknesses measured in the watersheds. In all cases our mean saturated thicknesses (4–4.5 m) are lower and compatible with measured



mean regolith thicknesses (4–6 m) on the watersheds. No regolith thickness measurements are available in P304, but the higher water storage determined by the hydrogeochemical modeling is consistent with the dampened hydrologic behavior and the higher base flow index in P304 (Safeeq and Hunsaker, 2016).

Little data are available for a direct comparison of modeled results in the Bull watersheds. However, the lower water storage and saturated thickness inferred from the geochemical modeling over three Bull watersheds (T003, B203, and B204) are consistent with previous studies in the region (e.g., Hubbert et al., 2001; Klos et al., 2018; O'Geen et al., 2018). By investigating plant-accessible water in mountain ecosystems, Klos et al. (2018) concluded that regolith thickness and water-storage capacity decrease with increasing elevation in the higher parts of the Sierra Nevada. Measured regolith thicknesses along the SSCZO elevation gradient (Figure 1) also show a trend of decreasing thickness from 2000 to 2700 m, with mean regolith thickness decreasing from 5 to 1.5 m between Providence and Short Hair (Short Hair on Figure 1; O'Geen et al., 2018). The lowest saturated thicknesses estimated by the hydrogeochemical modeling were located in the B203 and B204 watersheds, and corresponded to the lowest base flow indexes. Our modeling results using reactive-transport approaches and C-Q relations are therefore consistent with several independent estimates from hydrologic, geophysical and isotopic studies.

## The Control of CZ Structure on Hydrogeochemical Behavior in Headwater Catchments

The principal contribution of our study is to determine how CZ structure controls hydrogeochemical behavior and C-Q relations in headwater watersheds (Figure 12). We found that mean stream concentrations and heights of C-Q relations ( $a_{Ca2+}$  coefficient) are primarily controlled by regolith mineralogy and mean transit times of stream water (Figures 6B, 10). The control of regolith geochemistry on stream chemistry

is consistent with previous studies conducted at the KREW (Hunsaker and Johnson, 2017). Additionally, hydrogeochemical modeling indicates that the degree of chemodynamic behavior ( $b_{Ca2+}$  coefficient) is mainly controlled by the seasonal variability of mean transit times during dry periods (Figure 10). This seasonal variability itself is controlled by the geomorphologic features governing the water-storage capacity. Watersheds with thinner saturated thicknesses, a larger stream network and shorter subsurface flow lines have limited storage capacity and show limited variability of water transit times and chemostatic behaviors (e.g., B204, B203 in Figure 12). Watersheds with thicker saturated thicknesses and a more limited stream network have larger storage capacity and show higher variability of mean transit times and more chemodynamic behavior (e.g., B201, P304 in Figure 12).

The combination of chemostatic behavior with high mean stream water concentrations was not observed (section Hydrology and C-Q Relations), and this is explained by the fact that chemostatic behavior is caused by an absence of significant water storage, preventing the presence of waters with long transit times and high concentrations. This scheme is also consistent with the variability of water discharge and the base flow index (BFI, Table 2). The chemostatic watersheds clearly have hydrologic characteristics pointing to an absence of large water storage, with a high seasonal variability of water discharge and low BFI (Table 2). The chemodynamic watersheds show the opposite hydrologic characteristics, with low seasonal variability of stream discharge and a higher BFI (Table 2).

One of the important takeaways from this study is that the CZ structure in headwater watersheds matters more than their watershed areas for the understanding of hydrogeochemical behavior. For example, B203 has a watershed area that is 2.5 times the area of P304 (Table 2), however, its CZ structure with a thin saturated thickness, short subsurface flow lines and fast transit times generates low stream water concentrations and chemostatic behavior. P304 has higher water storage and longer transit times that generate high stream water concentrations and

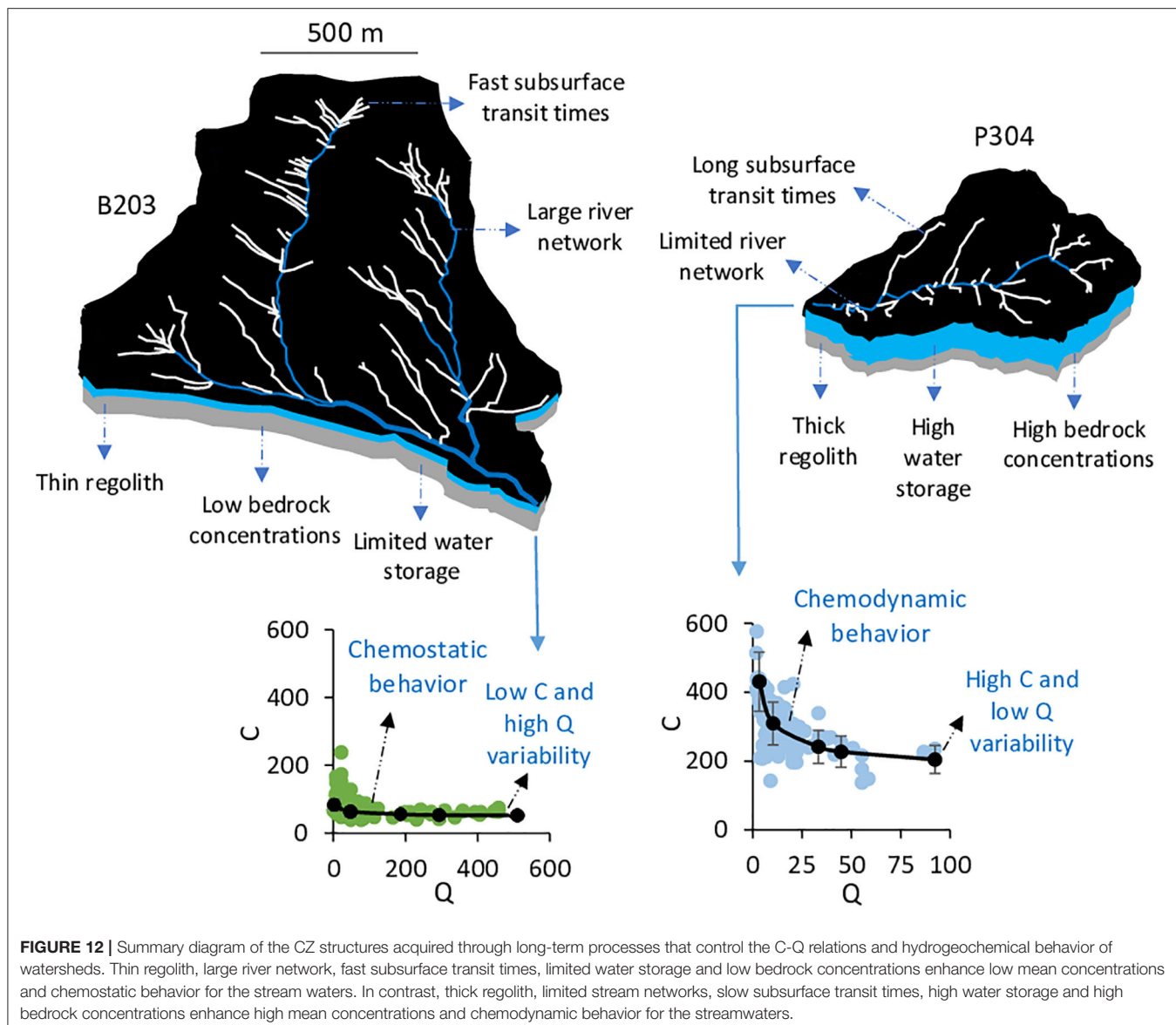


**FIGURE 12 |** Summary diagram of the CZ structures acquired through long-term processes that control the C-Q relations and hydrogeochemical behavior of watersheds. Thin regolith, large river network, fast subsurface transit times, limited water storage and low bedrock concentrations enhance low mean concentrations and chemostatic behavior for the stream waters. In contrast, thick regolith, limited stream networks, slow subsurface transit times, high water storage and high bedrock concentrations enhance high mean concentrations and chemodynamic behavior for the streamwaters.

chemodynamic behavior. These results suggest that the analysis and modeling of C-Q relations should not be done solely with surface-area-normalized stream discharge (e.g., Wymore et al., 2017; Zhi et al., 2019), as stream water chemistry is primarily controlled by the CZ structure and the distribution of subsurface flow lines, and not by watershed surface areas. At this stage, this point applies only for small headwater watersheds where our approach has been tested. The application of surface-area-normalized data cannot be evaluated with our study for larger watersheds (e.g., Moatar et al., 2017).

Since CZ structure constrains the shapes of C-Q relations, our study opens the possibility of estimating CZ attributes from existing C-Q data where the rich set of field investigations that we had are not available. For example, while combining data on regolith mineralogy with C-Q data from stream waters, the reactive-transport modeling of C-Q relations can be used to estimate water storage and water transit times. This point has

implications for using C-Q relations as a tool to estimate water storage and drought resistance.

We underline that these applications and implications hold when interpreting solutes in stream water with an important lithogenic origin, a strong C-MTT slope, and negative C-Q relations (C tend to decrease with Q, i.e.,  $\text{Ca}^{2+}$ ,  $\text{H}_4\text{SiO}_4$ , ...). Different strategies could be developed for other species with positive C-Q relations (C tend to increase with Q, i.e.,  $\text{NO}_3^-$ ,  $\text{SO}_4^{2-}$ ; Moatar et al., 2017). We expect that species with positive C-Q relations would not be explained in this way by the variability of transit times in the subsurface. Modeling positive C-Q relations could potentially be used to explore other processes in watersheds, such as remobilization processes from channels and soils, or interactions with the vegetation. This needs to be clearly tested in future studies with a specific focus on positive C-Q relations.

## Nature and Magnitude of Mixing Processes

A number of recent studies have debated the extent to which C-Q relations are controlled by mixing processes between different water sources (Liu et al., 2017; Torres et al., 2017; Zhi et al., 2019). In our study, the mixing of different subsurface waters occurs when subsurface flow lines reach the stream network (**Figure 2**). No mixing with deep groundwater or with tributary streams was needed to explain the chemical variability. The variability of transit times within the regolith and the mixing of different subsurface flow lines connected to the stream is sufficient to explain the C-Q relations. Our results support that at the small scale of headwater watersheds ( $0\text{--}2 \text{ km}^2$ ), stream chemistry and its variability are primarily controlled by the lateral flows within the regolith and the CZ structure controlling the architecture of the subsurface flow lines. The importance of lateral flows has been also highlighted in the modeling of geomorphic evolution of hills (Brantley et al., 2017).

At lower elevations in the Sierra Nevada and for larger watersheds ( $500\text{--}2,000 \text{ km}^2$ ), an influence from deep groundwater has been identified from the interpretation of C-Q relations from river waters (Liu et al., 2017). The magnitude of the deep-groundwater influence tends to increase when the elevation decreases and the river size increases (Liu et al., 2017). For major rivers, the mixing between different waters can be important when different tributaries draining contrasting lithologies are merged (Torres et al., 2017). Our results and the comparison with previous studies suggest that the nature and magnitude of mixing processes affecting C-Q relations depend to the river order from which water samples are coming. Complexity and contributions of mixing processes appear to increase from headwater streams to large-scale rivers.

In this study, we did not address the potential mixing of different waters coming from different vertical layers in the regolith. Vertically-averaged regolith properties, as used in this study, permit reduced computation times and the number of parameters in the model; however, this modeling approach cannot show the role of different regolith layers (i.e., superficial soil, soil base, lower saprolith) in the acquisition of C-Q relations. A potential improvement of our modeling strategy in future studies is a more detailed description of the CZ vertical heterogeneity and its incorporation in our modeling approach. This would imply that we either consider 2D cross-sections rather than 1D subsurface flow lines, or that we consider multiple subsurface flow lines distributed vertically with mixing between them. However, it is worth noting that this increase in model complexity would significantly increase the amount of field data needed to constrain the regolith physical, geochemical, and hydrologic properties for all the regolith layers in the KREW. In addition, our study did not evaluate the effect of direct input of snowmelt waters into the streams.

## Implications for Water Resources From Headwater Watersheds

This study, which was conducted along an elevation gradient of eight watersheds, has implications for understanding the

impact of droughts and hydrologic changes in a warmer climate. Presently, higher-elevation watersheds generate a greater fraction of runoff from the Sierra Nevada (Harrington and Bales, 1998; Meixner et al., 2004; Rice et al., 2011; Hunsaker et al., 2012). Our modeling results showed that higher-elevation watersheds (i.e., B203, B204) with thinner regolith and dilute stream chemistry have lower water-storage capacity and shorter water-transit times than the mid-elevation watersheds (i.e., P301, P303, P304). These results imply that in a warming climate with decreasing snowpacks, higher-elevation watersheds may not have sufficient storage capacity in the regolith to compensate for the water that is currently stored in snowpack during winter. Higher temperatures are also expected to produce larger flood events during the winter, followed by longer and drier summers with less runoff available for downstream users. This scenario of the future hydrologic response in the Sierra Nevada is consistent with previous studies investigating changes in runoff (Hunsaker et al., 2012), vegetation (Goulden and Bales, 2014) and flooding (Das et al., 2013). More broadly, mountain watersheds that experienced Pleistocene glaciations have been scoured by glacial and periglacial processes (Ackerer et al., 2016; Callahan et al., 2019), resulting in thinner regolith and potentially lower water-storage capacities. The CZ structure, which is acquired through long-term processes, may not be adaptable to the rapid changes in climate and snowpack that are currently being observed. This will change the hydrologic behavior of mountain watersheds and have implications for downstream storage capacity and operations.

## CONCLUSION

Detailed geomorphic analysis, characterization of C-Q relations and reactive-transport modeling from a unique elevation gradient determined how CZ structure controls hydrogeochemical behavior of watersheds. Our results indicate that (1) CZ attributes and structure are key determinants of C-Q relations (2) mean stream water concentrations and heights of C-Q relations are primarily controlled by the regolith mineralogy and mean transit times of subsurface water, and (3) the degree of chemodynamic behavior is very sensitive to the water-storage in watersheds. Watersheds with thinner regolith, larger stream networks and limited water storage have faster transit times along subsurface flow lines and show stream chemistry with limited seasonal variability (i.e., chemostatic behavior). In contrast, watersheds with thicker regolith, smaller stream networks and larger water storage have longer transit times along subsurface flow lines and exhibit greater chemical variability (i.e., chemodynamic behavior). No mixing with deep groundwater was needed to explain the chemical variability of stream water. Independent estimates of mean transit times and water-storage from other isotopic, hydrologic and geophysical studies were consistent with our results inferred from the modeling of C-Q relations. This study opens the possibility to estimate CZ characteristics such as water-storage capacity and mean transit times in headwater watersheds by using quantitative modeling of C-Q relations.

## DATA AVAILABILITY STATEMENT

All datasets generated for this study are included in the article/**Supplementary Material**.

## AUTHOR CONTRIBUTIONS

JA performed the majority of the research presented in this manuscript. CS was involved for the reactive-transport modeling. FL was involved for the chemical data and interpretation of C-Q relations. RBar was involved for the using of ArcGIS and DEM interpretation. MS was involved for the using of ArcGIS and DEM interpretation as well along with hydrometeorological data from KREW. AO'G was involved for regolith data, regolith thickness data, and mineralogical data. CH was involved for KREW data. RBal was involved for manuscript reading and re-writing and KREW data. All authors contributed to the article and approved the submitted version.

## REFERENCES

- Ackerer, J., Chabaux, F., Lucas, Y., Clément, A., Fritz, B., Beaulieu, E., et al. (2018). Monitoring and reactive-transport modeling of the spatial and temporal variations of the Strengbach spring hydrochemistry. *Geochim. Cosmochim. Acta* 225, 17–35. doi: 10.1016/j.gca.2018.01.025
- Ackerer, J., Chabaux, F., Van der Woerd, J., Viville, D., Pelt, E., Kali, E., et al. (2016). Regolith evolution on the millennial timescale from combined U–Th–Ra isotopes and in situ cosmogenic  $^{10}\text{Be}$  analysis in a weathering profile (Strengbach watershed, France). *Earth Planet. Sci. Lett.* 453, 33–43. doi: 10.1016/j.epsl.2016.08.005
- Ackerer, J., Jeannot, B., Delay, F., Weill, S., Lucas, Y., Fritz, B., et al. (2020). Crossing hydrological and geochemical modeling to understand the spatiotemporal variability of water chemistry in an elementary watershed (Strengbach, France). *Hydrol. Earth Syst. Sci.* 24, 3111–3133. doi: 10.5194/hess-24-3111-2020
- Ameli, A. A., Beven, K., Erlandsson, M., Creed, I. F., McDonnell, J. J., and Bishop, K. (2017). Primary weathering rates, water transit times, and concentration-discharge relations: A theoretical analysis for the critical zone. *Water Resour. Res.* 53, 942–960. doi: 10.1002/2016WR019448
- Bales, R. C., Goulden, M. L., Hunsaker, C. T., Conklin, M. H., Hartsough, P. C., O'Geen, A. T., et al. (2018). Mechanisms controlling the impact of multi-year drought on mountain hydrology. *Sci. Rep.* 8:690. doi: 10.1038/s41598-017-19007-0
- Bales, R. C., Hopmans, J. W., O'Geen, A. T., Meadows, M., Hartsough, P. C., Kirchner, P., et al. (2011). Soil moisture response to snowmelt and rainfall in a Sierra Nevada mixed-conifer forest. *Vadose Zone J.* 10, 786–799. doi: 10.2136/vzj2011.0001
- Bart, R., and Hope, A. (2014). Inter-seasonal variability in baseflow recession rates: the role of aquifer antecedent storage in central California watersheds. *J. Hydrol.* 519, 205–213. doi: 10.1016/j.jhydrol.2014.07.020
- Bateman, P. C., and Busacca, A. J. (1983). *Millerton Lake Quadrangle, Westcentral Sierra Nevada, California – Analytic Data*. US Geological Survey Professional Paper, Vol. 1261. Reston, VA: US Geological Survey. doi: 10.3133/pp1261
- Bateman, P. C., and Lockwood, J. P. (1976). *Shaver Lake Quadrangle, Westcentral Sierra Nevada, California – Analytic Data*. US Geological Survey Professional Paper, Vol. 774-D. Reston, VA: US Geological Survey. doi: 10.3133/pp774D
- Brantley, S. L., Lebedeva, M. I., Balashov, V. N., Singha, K., Sullivan, P. L., and Stinchcomb, G. (2017). Toward a conceptual model relating chemical reaction fronts to water flow paths in hills. *Geomorphology* 277, 100–117. doi: 10.1016/j.geomorph.2016.09.027
- Callahan, R. P., Ferrier, K. L., Dixon, J., Dosseto, A., Hahm, W. J., Jessup, B. S., et al. (2019). Arrested development: Erosional equilibrium in the southern Sierra Nevada, California, maintained by feedbacks between channel incision and hillslope sediment production. *GSA Bulletin* 131, 1179–1202. doi: 10.1130/B35006.1
- Chorover, J., Derry, L. A., and McDowell, W. H. (2017). Concentration–Discharge Relations in the Critical Zone: Implications for Resolving Critical Zone Structure, Function, and Evolution. *Water Resour. Res.* 53, 8654–8659. doi: 10.1002/2017WR021111
- Chorover, J., Troch, P. A., Rasmussen, C., Brooks, P. D., Pelletier, J. D., Breshears, D. D., et al. (2011). How water, carbon, and energy drive critical zone evolution: The Jemez–Santa Catalina Critical Zone Observatory. *Vadose Zone J.* 10, 884–899. doi: 10.2136/vzj2010.0132
- Das, T., Maurer, E. P., Pierce, D. W., Dettinger, M. D., and Cayan, D. R. (2013). Increases in flood magnitudes in California under warming climates. *J. Hydrol.* 501, 101–110. doi: 10.1016/j.jhydrol.2013.07.042
- Diamond, J. S., and Cohen, M. J. (2018). Complex patterns of watershed solute–discharge relationships for coastal plain rivers. *Hydrolog. Processes* 32, 388–401. doi: 10.1002/hyp.11424
- Gérard, F., Clement, A., and Fritz, B. (1998). Numerical validation of a Eulerian hydrochemical code using a 1D multisolute mass transport system involving heterogeneous kinetically controlled reactions. *J. Contam. Hydrol.* 30, 201–216. doi: 10.1016/S0169-7722(97)00047-8
- Godsey, S. E., Kirchner, J. W., and Clow, D. W. (2009). Concentration–discharge relationships reflect chemostatic characteristics of US watersheds. *Hydrolog. Processes* 23, 1844–1864. doi: 10.1002/hyp.7315
- Goulden, M. L., Anderson, R. G., Bales, R. C., Kelly, A. E., Meadows, M., and Winston, G. C. (2012). Evapotranspiration along an elevation gradient in California's Sierra Nevada. *J. Geophys. Res.* 117:G3. doi: 10.1029/2012JG002027
- Goulden, M. L., and Bales, R. C. (2014). Mountain runoff vulnerability to increased evapotranspiration with vegetation expansion. *Proc. Natl. Acad. Sci.* 111, 14071–14075. doi: 10.1073/pnas.1319316111
- Harrington, R., and Bales, R. C. (1998). Modeling ionic solute transport in melting snow. *Water Resour. Res.* 34, 1727–1736. doi: 10.1029/98WR00557
- Herndon, E. M., Dere, A. L., Sullivan, P. L., Norris, D., Reynolds, B., and Brantley, S. L. (2015). Landscape heterogeneity drives contrasting concentration–discharge relationships in shale headwater watersheds. *Hydrol. Earth Syst. Sci.* 19, 3333–3347. doi: 10.5194/hess-19-3333-2015
- Herndon, E. M., Steinhofel, G., Dere, A. L., and Sullivan, P. L. (2018). Perennial flow through convergent hillslopes explains chemodynamic solute behavior in a shale headwater watershed. *Chem. Geol.* 493, 413–425. doi: 10.1016/j.chemgeo.2018.06.019
- Holbrook, W. S., Riebe, C. S., Elwaseif, M. L., Hayes, J., Basler-Reeder, K., Harry, D. L., et al. (2014). Geophysical constraints on deep weathering and water storage

## FUNDING

This study was supported by the U.S. National Science Foundation (NSF) through the Southern Sierra Critical Zone Observatory (EAR-0725097). This research was also supported by the long-term collaborations with the Pacific Southwest Research Station and the U.S Forest Service. CS was supported by the Watershed Function Science Focus Area at Lawrence Berkeley National Laboratory funded by the U.S. Department of Energy, Office of Science, Biological and Environmental Research under Contract No. DE-AC02-05CH11231.

## SUPPLEMENTARY MATERIAL

The Supplementary Material for this article can be found online at: <https://www.frontiersin.org/articles/10.3389/frwa.2020.00023/full#supplementary-material>

- potential in the Southern Sierra Critical Zone Observatory. *Earth Surface Processes Landforms* 39, 366–380. doi: 10.1002/esp.3502
- Hubert, K. R., Beyers, J. L., and Graham, R. C. (2001). Roles of weathered bedrock and soil in seasonal water relations of *Pinus jeffreyi* and *Arctostaphylos patula*. *Can. J. Forest Res.* 31, 1947–1957. doi: 10.1139/x01-136
- Hunsaker, C. T., and Johnson, D. W. (2017). Concentration-discharge relationships in headwater streams of the Sierra Nevada, California. *Water Resour. Res.* 53, 7869–7884. doi: 10.1002/2016WR019693
- Hunsaker, C. T., Whitaker, T. W., and Bales, R. C. (2012). Snowmelt runoff and water yield along elevation and temperature gradients in California's southern Sierra Nevada 1. *J. Am. Water Res. Association* 48, 667–678. doi: 10.1111/j.1752-1688.2012.00641.x
- Jessup, B. S., Jesse Hahn, W., Miller, S. N., Kirchner, J. W., and Riebe, C. S. (2011). Landscape response to tipping points in granite weathering: The case of stepped topography in the Southern Sierra Critical Zone Observatory. *Appl. Geochem.* 26, S48–S50. doi: 10.1016/j.apgeochem.2011.03.026
- Johnson, D. W., Hunsaker, C. T., Glass, D. W., Rau, B. M., and Roath, B. A. (2011). Carbon and nutrient contents in soils from the Kings River Experimental Watersheds, Sierra Nevada Mountains, California. *Geoderma* 160, 490–502. doi: 10.1016/j.geoderma.2010.10.019
- Kim, H., Dietrich, W. E., Thurnhoffer, B. M., Bishop, J. K., and Fung, I. Y. (2017). Controls on solute concentration-discharge relationships revealed by simultaneous hydrochemistry observations of hillslope runoff and stream flow: The importance of critical zone structure. *Water Resour. Res.* 53, 1424–1443. doi: 10.1002/2016WR019722
- Klos, P. Z., Goulden, M. L., Riebe, C. S., Tague, C. L., O'Geen, A. T., Flinchum, B. A., et al. (2018). Subsurface plant-accessible water in mountain ecosystems with a Mediterranean climate. *Wiley Interdiscipl. Rev.* 5:e1277. doi: 10.1002/wat2.1277
- Lackey, J. S., Cecil, M. R., Windham, C. J., Frazer, R. E., Bindeman, I. N., and Gehrels, G. E. (2012). The Fine Gold intrusive suite: the roles of basement terranes and magma source development in the Early Cretaceous Sierra Nevada batholith. *Geosphere* 8, 292–313. doi: 10.1130/GES00745.1
- Li, L., Bao, C., Sullivan, P. L., Brantley, S., Shi, Y., and Duffy, C. (2017). Understanding watershed hydrogeochemistry: 2. Synchronized hydrologic and geochemical processes drive stream chemostatic behavior. *Water Res. Res.* 53, 2346–2367. doi: 10.1002/2016WR018935
- Liu, F., Conklin, M. H., and Shaw, G. D. (2017). Insights into hydrologic and hydrochemical processes based on concentration-discharge and end-member mixing analyses in the mid-Merced River Basin, Sierra Nevada, California. *Water Resour. Res.* 53, 832–850. doi: 10.1002/2016WR019437
- Liu, F., Hunsaker, C., and Bales, R. C. (2013). Controls of streamflow generation in small watersheds across the snow-rain transition in the Southern Sierra Nevada, California. *Hydrolog. Processes* 27, 1959–1972. doi: 10.1002/hyp.9304
- Liu, Y. B., Gebremeskel, S., De Smedt, F., Hoffmann, L., and Pfister, L. (2003). A diffusive transport approach for flow routing in GIS-based flood modeling. *J. Hydrol.* 283, 91–106. doi: 10.1016/S0022-1694(03)00242-7
- Lucas, Y., Chabaux, F., Schaffhauser, T., Fritz, B., Ambroise, B., Ackerer, J., et al. (2017). Hydrogeochemical modeling (KIRMAT) of spring and deep borehole water compositions in the small granitic Ringelbach watershed (Vosges Mountains, France). *Appl. Geochem.* 87, 1–21. doi: 10.1016/j.apgeochem.2017.10.005
- Meixner, T., Gutmann, C., Bales, R., Leydecker, A., Sickman, J., Melack, J., et al. (2004). Multidecadal hydrochemical response of a Sierra Nevada watershed: sensitivity to weathering rate and changes in deposition. *J. Hydrol.* 285, 272–285. doi: 10.1016/j.jhydrol.2003.09.005
- Moatar, F., Abbott, B. W., Minaudo, C., Curie, F., and Pinay, G. (2017). Elemental properties, hydrology, and biology interact to shape concentration-discharge curves for carbon, nutrients, sediment, and major ions. *Water Resour. Res.* 53, 1270–1287. doi: 10.1002/2016WR019635
- Musolff, A., Schmidt, C., Selle, B., and Fleckenstein, J. H. (2015). Catchment controls on solute export. *Adv. Water Resour.* 86, 133–146. doi: 10.1016/j.advwatres.2015.09.026
- Ngo, V. V., Delalande, M., Clément, A., Michau, N., and Fritz, B. (2014). Coupled transport-reaction modeling of the long-term interaction between iron, bentonite and Callovian-Oxfordian claystone in radioactive waste confinement systems. *Appl. Clay Sci.* 101, 430–443. doi: 10.1016/j.clay.2014.08.020
- O'Geen, A. T., Safeeq, M., Wagenbrenner, J., Stacy, E., Hartsough, P., Devine, S., et al. (2018). Southern Sierra Critical Zone Observatory and Kings River experimental watersheds: a synthesis of measurements, new insights, and future directions. *Vadose Zone J.* 17:81. doi: 10.2136/vzj2018.04.0081
- Reis, F. D. A., and Brantley, S. L. (2019). The impact of depth-dependent water content on steady state weathering and eroding systems. *Geochim. Cosmochim. Acta* 244, 40–55. doi: 10.1016/j.gca.2018.09.028
- Rice, R., Bales, R. C., Painter, T. H., and Dozier, J. (2011). Snow water equivalent along elevation gradients in the Merced and Tuolumne River basins of the Sierra Nevada. *Water Resour. Res.* 47:8. doi: 10.1029/2010WR009278
- Safeeq, M., Grant, G. E., Lewis, S. L., and Tague, C. L. (2013). Coupling snowpack and groundwater dynamics to interpret historical streamflow trends in the western United States. *Hydrolog. Processes* 27, 655–668. doi: 10.1002/hyp.9628
- Safeeq, M., and Hunsaker, C. T. (2016). Characterizing runoff and water yield for headwater watersheds in the southern Sierra Nevada. *J. Am. Water Res. Association* 52, 1327–1346. doi: 10.1111/1752-1688.12457
- Steefel, C. I., Appelo, C. A. J., Arora, B., Jacques, D., Kalbacher, T., Kolditz, O., et al. (2015). Reactive transport codes for subsurface environmental simulation. *Comp. Geosci.* 19, 445–478. doi: 10.1007/s10596-014-9443-x
- Storck, P., Bowling, L., Wetherbee, P., and Lettenmaier, D. (1998). Application of a GIS-based distributed hydrology model for prediction of forest harvest effects on peak stream flow in the Pacific Northwest. *Hydrolog. Process* 12, 889–904.
- Sullivan, P. L., Stops, M. W., Macpherson, G. L., Li, L., Hirnmas, D. R., and Dodds, W. K. (2019). How landscape heterogeneity governs stream water concentration-discharge behavior in carbonate terrains (Konza Prairie, USA). *Chem. Geol.* 527:118989. doi: 10.1016/j.chemgeo.2018.12.002
- Tardy, Y., and Fritz, B. (1981). An ideal solid solution model for calculating solubility of clay minerals. *Clay Minerals* 16, 361–373. doi: 10.1180/claymin.1981.016.4.05
- Tian, Z., Hartsough, P. C., and O'Geen, A. T. (2019). Lithologic, climatic and depth controls on critical zone transformations. *Soil Sci. Soc. Am. J.* 83, 437–447. doi: 10.2136/sssaj2018.03.0120
- Torres, M. A., Baronas, J. J., Clark, K. E., Feakins, S. J., and West, A. J. (2017). Mixing as a driver of temporal variations in river hydrochemistry: 1. Insights from conservative tracers in the Andes-Amazon transition. *Water Res. Res.* 53, 3102–3119. doi: 10.1002/2016WR019733
- Visser, A., Thaw, M., Deinhart, A., Bibby, R., Safeeq, M., Conklin, M., et al. (2019). Cosmogenic isotopes unravel the hydrochronology and water storage dynamics of the Southern Sierra Critical Zone. *Water Resour. Res.* 55, 1429–1450. doi: 10.1029/2018WR023665
- Wymore, A. S., Brereton, R. L., Ibarra, D. E., Maher, K., and McDowell, W. H. (2017). Critical zone structure controls concentration-discharge relationships and solute generation in forested tropical montane watersheds. *Water Resour. Res.* 53, 6279–6295. doi: 10.1002/2016WR020016
- Zhi, W., Li, L., Dong, W., Brown, W., Kaye, J., Steefel, C., et al. (2019). Distinct source water chemistry shapes contrasting concentration-discharge patterns. *Water Resour. Res.* 55, 4233–4251. doi: 10.1029/2018WR024257

**Conflict of Interest:** The authors declare that the research was conducted in the absence of any commercial or financial relationships that could be construed as a potential conflict of interest.

Copyright © 2020 Ackerer, Steefel, Liu, Bart, Safeeq, O'Geen, Hunsaker and Bales. This is an open-access article distributed under the terms of the Creative Commons Attribution License (CC BY). The use, distribution or reproduction in other forums is permitted, provided the original author(s) and the copyright owner(s) are credited and that the original publication in this journal is cited, in accordance with accepted academic practice. No use, distribution or reproduction is permitted which does not comply with these terms.